TEKNILLINEN KORKEAKOULU
Teknillisen Fysiikan ja
Matematiikan Osasto

Teijo Lehtinen

DC SQUID Microwave Amplifier

Master's Thesis submitted in partial fulfillment of the
requirements for the degree of Master of Science in
Technology

Espoo, November 16, 2004

Supervisor : Professor Pekka Hautojärvi
Instructor : Professor Pertti Hakonen

Helsinki University of Technology
Department of Engineering Physics and Mathematics

ABSTRACT OF
MASTER'S THESIS

Author	Teijo Lehtinen
Department	Department of Engineering Physics and Mathematics
Major subject	Physics
Minor subject	Engineering Physics, Advanced Energy Systems
Title	DC SQUID Microwave Amplifier
Title in Finnish	DC SQUID Mikroaaltovahvistin
Chair	Tfy-3 Physics
Supervisor	Professor Pekka Hautojärvi
Instructor	Professor Pertti Hakonen

Abstract

The noise performance of a DC SQUID amplifier cooled to subkelvin temperatures is, at best, quantum limited: at gigahertz frequencies, the input noise temperature can be just a few tens of millikelvins. Such a noise temperature is unreachable with any other known microwave amplifier technologies.

In this Master's Thesis, a state-of-the-art DC SQUID microwave amplifier, LTL 800, fabricated in Technical Research Centre of Finland (VTT), was completely characterized both experimentally and theoretically.

The operation principles were studied by constructing an analytical model of the device, and the experimental results were successfully explained by a detailed circuit simulation model. Both of the models will be applied in designing forthcoming SQUID amplifiers.

The gain of LTL 800 SQUID amplifier was measured to be 22 dB at 630 MHz with 150 MHz bandwidth. The gain-bandwidth product, 24 GHz, is superior compared with the results achieved by any other manufacturer. We obtained a 5.5 K input noise temperature at 4.2 Kelvin bath temperature. According to the experimental results and simulations, at a 50 mK bath temperature, the noise temperature can be expected to be 150 mK, which is a factor of three larger than the quantum limit.

Number of pages	55	**Key words**	DC SQUID, low noise amplifier, high frequency amplifier, superconducting electronics

Department fills

Approved   **Library code**

Teknillinen korkeakoulu
Teknillisen fysiikan ja matematiikan osasto

DIPLOMITYÖN
TIIVISTELMÄ

Tekijä	Teijo Lehtinen
Osasto	Teknillisen fysiikan ja matematiikan osasto
Pääaine	Fysiikka
Sivuaine	Teknillinen fysiikka, energiateknologiat
Työn nimi	DC SQUID Mikroaaltovahvistin
Title in English	DC SQUID Microwave Amplifier
Professuurin koodi ja nimi	Tfy-3 Fysiikka
Työn valvoja	Professori Pekka Hautojärvi
Työn ohjaaja	Professori Pertti Hakonen

Tiivistelmä

Alle Kelvinin lämpötilaan jäähdytetyn DC SQUID vahvistimen kohina on parhaimmillaan kvanttirajoitteista: gigahertsin taajuuksilla sisääntulokohinalämpötila voi olla vain muutamia kymmeniä millikelvenejä. Vastaaviin kohinalämpötiloihin on mahdotonta päästä millään muulla tunnetulla vahvistin tyypillä.

Tässä diplomityössä karakterisoitiin uusinta tekniikkaa edustava DC SQUID mikroaaltovahvistin, LTL 800. Laite on valmistettu Valtion teknillisessä tutkimuslaitoksessa (VTT).

Toimintaperiaatteiden ymmärtämiseksi kehitimme analyyttisen mallin laitteesta, ja mittaustulokset onnistuttiin selittämään yksityiskohtaisella piirisimulaatiomallilla. Molempia malleja tullaan soveltamaan uusien SQUID vahvistimien suunnitteluun.

LTL 800 SQUID vahvistimen vahvistukseksi mitattiin 22 dB taajuudella 630 MHz ja 150 MHz:n taajuuskaistalla. Vahvistus-kaista tulo, 24 GHz, on erinomainen muiden valmistajien tuloksiin verrattuna. Sisääntuloon ekvivalentiksi kohinalämpötilaksi saatiin 5,5 Keiviniä 4,2 Kelvinin mittauslämpötilassa. Mittaustulosten ja simulaatioiden perusteella vahvistimen kohinalämpötilaksi 50 mK:n mittauslämpötilassa voidaan arvioida 150 mK, joka on vain kertoimella kolme suurempi kuin kvanttiraja.

Sivumäärä	55	Avainsanat	DC SQUID, pienikohinainen vahvistin, korkeataajuusvahvistin, suprajohtava elektroniikka

Täytetään osastolla
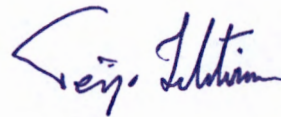Hyväksytty   **Kirjasto**

Contents

Preface

My earlier research experience was far from nanophysics at the time I started my Master's Thesis project in Nano research group in Low Temperature Laboratory, but with Professor Pertti Hakonen's excellent guidance the learning process have been both expeditious and exciting. I am grateful to Professor Hakonen and Professor Mikko Paalanen, the head of the laboratory, for the opportunity to participate in this honorable research unit.

I want to thank Ph.D Jari S. Penttilä, who has been the main designer behind LTL 800 SQUID amplifier. The computer simulation model, and many analytical ideas are originally his handicrafts.

I am also thankful to M.Sc Mika Sillanpää and Ph.D Leif Roschier who assisted me with the experimental studies, and M.Sc René Lindell who offered his valuable time for proof-reading and commenting the written work. I would also like to thank the inspiring conversations with Professor Bill Graham from Queen's University of Belfast.

Lastly, I want to express my gratitude to my parents, relatives, and friends, who have always supported my studies, and who have made my life delightful.

Otaniemi, 16 November, 2004   Teijo Lehtinen

Chapter 1

Introduction

Superconducting QUantum Interface Device, SQUID, is the most useful super-conducting instrument developed so far. There are numerous variants of SQUIDs, of which the so called DC SQUIDs have dominated the field of applications. The DC SQUID is the most sensitive magnetometer known. They have been applied widely in experimental research including the detection of gravitational waves, nuclear magnetic resonance, noise, radiation, and biomagnetic fields. Conventionally, the DC SQUIDs have been used only for low frequency applications, but with careful design, the operation frequencies can be extended to the microwave range.

The property that makes a DC SQUID based microwave amplifier highly interesting is its outstanding noise performance: the theoretical quantum limit of the input noise temperature is only a few tens of millikelvins at gigahertz frequencies. Recent studies have demonstrated that the quantum limit can be reached by cooling a high quality SQUID amplifier down to subkelvin temperatures [1]. Such noise temperatures are unreachable with any other known microwave amplifier technologies. The best competitor, a high electron mobility transistor (HEMT) cooled to liquid ^{4}He temperatures is limited to noise temperatures of the order of a few Kelvins. Additionally, the power dissipation of the DC SQUIDs is extremely low, a few picowatts, while the HEMT amplifiers dissipate several milliwatts. Dissipated power heats the surrounding environment, which may be disastrous, for example, in superconducting electronics.

In this Master's Thesis, a state-of-the-art DC SQUID microwave amplifier, LTL 800, fabricated in Technical Research Centre of Finland (VTT), has been studied both experimentally and theoretically. Particularly, the noise performance and the microwave characteristics have been determined in a wide range of operation points using a spectrum analyzer and a vector network analyzer. To understand the behavior of the device, we constructed an analytical model

based on lumped circuit elements. Furthermore, a detailed computer simulation model, originally written for the design process, was improved to explain the rather unexpected experimental results. Both of the models will be applied for future SQUID amplifier designs.

The organization of the work is the following. In Chapter 2, we review the basics of the DC SQUID. The circuitry and the parameter values of the test device, are considered in Chapter 3. The analytical circuit model of the DC SQUID amplifier is derived in Chapter 4, and the computer simulation model is described in Chapter 5. In Chapter 6 we show the experimental configurations. The main experimental results, and the corresponding results from the computer simulations, are presented and analyzed in Chapter 7. The work is concluded briefly in Chapter 8.

Chapter 2

DC SQUID

In this chapter we will give a qualitative description of the DC SQUID starting from a simple derivation of the Josephson equations. The main goal is to understand the current-voltage characteristics, as well as, the flux-to-voltage and flux-to-current transfer functions. Similar derivations can be found from [2–4].

2.1 Josephson Equations

According to the microscopic theory of superconductivity, there exists an attractive interaction between the electrons in a superconductor resulting bound states of electrons. These two electron quasiparticles are called Cooper pairs. The extent of a Cooper pair is much greater than the average separation of electrons. In fact, in the region of a single pair there are millions of electrons, which are themselves correlated into pairs. This macroscopic correlation results that all Cooper pairs in a superconductor can be presented by a single wave function, the Ginzburg-Landau order parameter:

$$\psi(\mathbf{r}) = |\psi(\mathbf{r})|e^{i\varphi(\mathbf{r})}. \tag{2.1}$$

Here $|\psi|^2$ can be identified as the density of Cooper pairs and φ is the phase of the state. The long range order fixes the value of the phase in all points in the superconductor.

The current density of Cooper pairs with charge $-2e$ and mass $2m_e$ can be written as [1]

$$\mathbf{J} = \frac{ie\hbar}{2m_e}\left(\psi^*\nabla\psi - \psi\nabla\psi^*\right) - \frac{2e^2}{m_e}\psi^*\psi\mathbf{A}, \tag{2.2}$$

where $\mathbf{A}$ is the magnetic vector potential. Inserting the order parameter (2.1) leads to

$$\mathbf{J} = -\frac{e\hbar}{m_e}|\psi|^2\left(\nabla\varphi + \frac{2\pi}{\Phi_0}\mathbf{A}\right), \tag{2.3}$$

where $\Phi_0 \equiv h/2e$ is the flux quantum. Thus, the gradient of the phase φ determines the current carrying states in the superconductor.

There is a nonzero probability for a quantum mechanical particle to tunnel through a thin, classically impenetrable, energy barrier. Tunneling of Cooper pairs through a region in which the superconductivity is weakened gives rise to the Josephson effect. The region is called a weak link, and it can be a point contact, a normal metal layer, or an insulating layer.

The Josephson effect can be understood qualitatively by assuming that the Cooper pair density decays exponentially within an insulating layer with a decay constant α [2]. If two identical superconductors k=1,2, with GL wave functions

$$\psi_k = |\psi|_\infty e^{i\varphi_k}, \tag{2.4}$$

where $|\psi|_\infty$ refers to the Cooper pair densities deep inside the superconductors, are separated by a thin insulating layer, the superposition of the two wave functions can be written as

$$\psi_k = |\psi|_\infty\left(e^{i\varphi_1 - \alpha(x+l/2)} + e^{i\varphi_2 + \alpha(x-l/2)}\right), \tag{2.5}$$

where l is the thickness of the tunnel barrier. Neglecting magnetic field and inserting (2.5) into (2.2) we get the first Josephson equation

$$J = \frac{ie\hbar}{m_e}|\psi|_\infty^2\alpha e^{-\alpha l}\left(e^{i(\varphi_2-\varphi_1)} - e^{-i(\varphi_2-\varphi_1)}\right) = J_c\sin\Delta\varphi, \tag{2.6}$$

where the critical current, J_c, is the maximum supercurrent density that the junction supports, and $\Delta\varphi$ is the difference in the phase between the two electrodes. Equation (2.6) introduces the DC Josephson effect, which predicts that if there is a difference in phase between the superconductors connected by a weak link, a

---

[1]Semiclassically, the canonical momentum of a particle with mass $2m_e$ and charge $-2e$ is $\mathbf{p} = 2m\mathbf{v} - 2e\mathbf{A}$, from which the average velocity of the particle is $\langle\mathrm{Re}(\hat{\mathbf{v}})\rangle = \frac{1}{2}\langle\mathbf{v} + \mathbf{v}^*\rangle = \frac{1}{4m^*}\langle\psi|\left((\hat{\mathbf{p}} + 2e\mathbf{A}) + (\hat{\mathbf{p}} + 2e\mathbf{A})^*\right)|\psi\rangle = \frac{-i\hbar}{4m}\left(\psi^*\nabla\psi - \psi\nabla\psi^*\right) + \frac{e}{m}\mathbf{A}\psi^*\psi$. The current density is then $J = -2e\langle\mathrm{Re}(\hat{\mathbf{v}})\rangle$.

supercurrent of Cooper pairs flows across the junction even in the absence of an applied electric field.

The time evolution of a quantum mechanical state in stationary potential is described by the Schrödinger equation

$$i\hbar \frac{\partial \psi}{\partial t} = E\psi. \tag{2.7}$$

Inserting the GL wave function (2.4) into (2.7) gives

$$-\hbar \psi_k \frac{\partial \varphi_k}{\partial t} = E_k \psi_k, k = 1, 2. \tag{2.8}$$

The transfer of a pair of electrons from one side of a Josephson tunnel junction to the other involves an energy $E = -2eV$, where V is the voltage applied over the junction. Subtracting equations (2.8) from each other, and writing $\varphi_2 - \varphi_1 \equiv \Delta\varphi$, leads to

$$\frac{d\Delta\varphi}{dt} = \frac{2eV}{\hbar}, \tag{2.9}$$

which is the second Josephson equation characterizing the AC Josephson effect. If we integrate equation (2.9) from $t = 0$ to t, and substitute the result into the first Josephson equation (2.6), we get

$$J(t) = J_c \sin\left(\frac{2eV}{\hbar}t + \Delta\varphi(0)\right). \tag{2.10}$$

Thus, application of a DC voltage across the Josephson junction produces an alternating current with the frequency

$$f_J = \frac{2eV}{h}, \tag{2.11}$$

which is called the Josephson frequency.

The phase difference, $\Delta\varphi$, is not gauge invariant, and therefore it cannot determine any physical quantity, such as the current density. A phase difference that is independent of the selection of gauge is

$$\gamma = \Delta\varphi - \frac{2\pi}{\Phi_0} \int_a^b \mathbf{A} \cdot d\mathbf{s}, \tag{2.12}$$

where the integration is from one electrode of the junction to the other. Using the gauge-invariant phase difference, the Josephson relations can be written as

$$J = J_c \sin(\gamma), \tag{2.13}$$

and

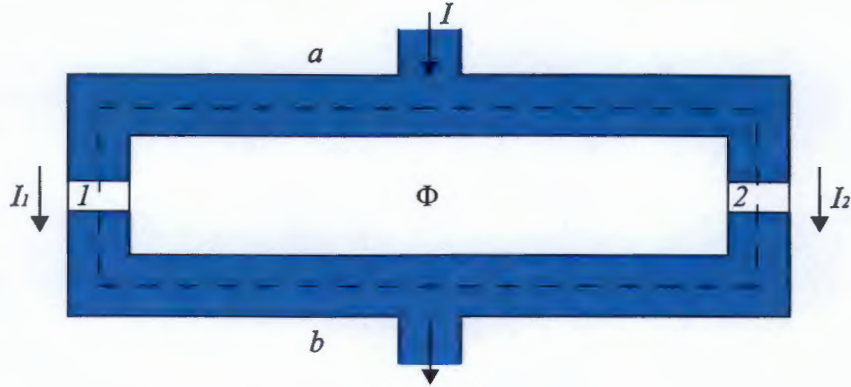$$\frac{d\gamma}{dt} = \frac{2eV}{\hbar}. \tag{2.14}$$

Figure 2.1: A schematic figure of the DC SQUID consisting of a superconducting loop interrupted by two Josephson junctions.

2.2 Critical Current

The DC SQUID is basically a superconducting ring interrupted by two weak links as depicted in figure 2.1. The line integral of the vector potential **A** around a contour passing through the junctions 1 and 2 and the electrodes a and b gives the enclosed flux Φ:

$$\Phi = \oint \mathbf{A} \cdot d\mathbf{s} = \int_1 \mathbf{A} \cdot d\mathbf{s} + \int_2 \mathbf{A} \cdot d\mathbf{s} + \int_a \mathbf{A} \cdot d\mathbf{s} + \int_b \mathbf{A} \cdot d\mathbf{s}. \qquad (2.15)$$

In the bulk superconductor, the superconducting current is zero,[2] and equation (2.3) reduces to $\mathbf{A} = (\Phi_0/2\pi)\nabla\varphi$. Selecting an integration path deep inside the superconducting electrodes, we can write

$$\int_a \mathbf{A} \cdot d\mathbf{s} + \int_b \mathbf{A} \cdot d\mathbf{s} = \frac{\Phi_0}{2\pi}\left(\int_a \nabla\varphi \cdot d\mathbf{s} + \int_b \nabla\varphi \cdot d\mathbf{s}\right) = \frac{\Phi_0}{2\pi}(\Delta\varphi_a + \Delta\varphi_b), \ (2.16)$$

where $\Delta\varphi_a$ and $\Delta\varphi_b$ are the phase differences across the electrodes a and b, respectively. Using equation (2.12), we get

$$\int_1 \mathbf{A} \cdot d\mathbf{s} + \int_2 \mathbf{A} \cdot d\mathbf{s} = \frac{\Phi_0}{2\pi}\left(\gamma_2 - \gamma_1 + \Delta\varphi_1 + \Delta\varphi_2\right), \qquad (2.17)$$

where γ_1 and γ_2 are the gauge-invariant phase differences (defined from the electrode a to the electrode b), and $\Delta\varphi_1$ and $\Delta\varphi_2$ are the phase differences across

---

[2]The Meissner effect implies that a weak magnetic field decays exponentially in the superconductor, and hence, according to the Maxwell equation $\mathbf{J} \propto \nabla \times \mathbf{H}$, the supercurrent vanishes.

the junctions 1 and 2, respectively. Since the phase must be single-valued, the total phase change across the loop must be a multiple of 2π, i.e.

$$\Delta\varphi_a + \Delta\varphi_b + \Delta\varphi_1 + \Delta\varphi_2 = n2\pi. \tag{2.18}$$

Combining equations (2.15), (2.16), (2.17) and (2.18), and setting $n = 0$, we get the relation between the gauge invariant phase differences:

$$\gamma_1 - \gamma_2 = \frac{2\pi\Phi}{\Phi_0}. \tag{2.19}$$

The total flux enclosed by the loop, Φ, is the sum of the external applied flux Φ_x and the flux induced by the screening supercurrent,

$$I_s = \frac{1}{2}(I_2 - I_1), \tag{2.20}$$

circulating in the loop. If the loop inductance is L, the self induced flux is

$$\Phi_s = LI_s. \tag{2.21}$$

Now, relation (2.19) becomes

$$\gamma_1 - \gamma_2 = \frac{2\pi}{\Phi_0}\left(\Phi_x + \frac{1}{2}L(I_2 - I_1)\right). \tag{2.22}$$

Assuming identical junctions[3] with a critical current I_c, and substituting the first Josephson equation (2.13) gives

$$\gamma_1 - \gamma_2 = \frac{2\pi}{\Phi_0}\left(\Phi_x + \frac{1}{2}LI_c(\sin\gamma_2 - \sin\gamma_1)\right). \tag{2.23}$$

The total supercurrent flowing through the SQUID circuit is

$$I = I_1 + I_2 = I_c(\sin\gamma_1 + \sin\gamma_2). \tag{2.24}$$

The maximum current that can flow across the SQUID without resistance with given Φ_x is found by solving γ_2 numerically from the implicit relation 2.23, and maximizing (2.20) with respect to γ_1. Alternatively, we can formally substitute equation (2.19) into equation (2.24) to get

$$I = I_c\left(\sin\gamma_1 + \sin\left(\gamma_1 - \frac{2\pi\Phi}{\Phi_0}\right)\right), \tag{2.25}$$

---

[3]A DC SQUID with somewhat asymmetrical junctions exhibits only slightly different properties [8].
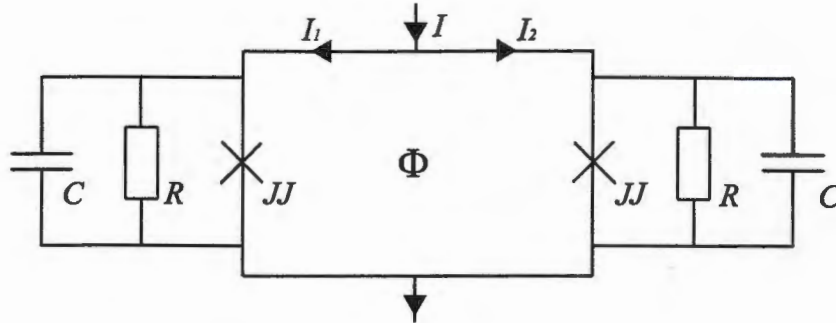
Figure 2.2: The resistively and capacitively shunted junction model of the DC SQUID.

which is easy to maximize with respect to γ_1, and the result is

$$I_m = 2I_c \left| \cos\left(\frac{\pi\Phi}{\Phi_0}\right) \right|. \tag{2.26}$$

The SQUID critical current is thus a periodic function of the total flux, Φ, enclosed by the loop with a period of one flux quantum. According to equation (2.26), the maximum supercurrent is zero at $\Phi = (n + 1/2)\Phi_0$. The screening currents try to keep Φ at multiplies of the flux quantum, and since the minimum circulating current is energetically advantageous, a step change of Φ_s occurs at $(n+1/2)\Phi_0$ [4]. Hence, the self induced flux effectively just increases the minimum critical current, but maintains the fundamental Φ_0-periodicity.

2.3   Electrical Equivalent Model

The Josephson equations describe properly the behavior of a large Josephson junction[4] with current below the critical current. The characteristics of the large Josephson junction in the finite voltage region can be explained by the Resistively and Capacitively Shunted Junction (RCSJ) model.

The RCSJ-model of the DC SQUID is depicted in Figure 2.2. In the case of the SQUID amplifiers considered in this work, the junctions are shunted by real resistances R. For tunnel junctions, the capacitance C is approximately the capacitance characterized by the barrier thickness and dielectric constant.

---

[4]Here the large junction means that the current can be considered as a flow of continuous charge density instead of discrete charge carriers.

The total current I through the SQUID is the sum of the loop currents:

$$I = I_1 + I_2. \tag{2.27}$$

In the model, the Josephson junctions are described by the ideal Josephson equations (2.13) and (2.14), in which case the loop currents, I_1 and I_2, are simply

$$I_i = I_c \sin \gamma_i + \frac{V}{R} + C \frac{dV}{dt} + I_{ni}, \qquad i = 1, 2, \tag{2.28}$$

where I_{ni} is the noise current from the shunt resistor. We can eliminate V from (2.28) by substituting the second Josephson equation (2.14) to obtain

$$\frac{I_i}{I_c} = \frac{\Phi_0 C}{2\pi I_c} \frac{d^2 \gamma_i}{dt^2} + \frac{\Phi_0}{2\pi R I_c} \frac{d\gamma_i}{dt} + \sin \gamma_i + \frac{I_{ni}}{I_c}. \tag{2.29}$$

Changing into a dimensionless time variable $\theta \equiv 2\pi I_c R t / \Phi_0$ leads to

$$\frac{I_i}{I_c} = \beta_c \frac{d^2 \gamma_i}{d\theta^2} + \frac{d\gamma_i}{d\theta} + \sin \gamma_i + \frac{I_{ni}}{I_c}, \tag{2.30}$$

where we have introduced the Stewart-McCumber damping parameter

$$\beta_C = \frac{2\pi I_c R^2 C}{\Phi_0}. \tag{2.31}$$

Combining equations (2.22), (2.27), and (2.30), and substituting variables $\nu = (\gamma_1 + \gamma_2)/2$, $\phi = (\gamma_1 - \gamma_2)/2$, $\phi_a = \pi \Phi_a / \Phi_0$ and $i = I/2I_c$ we get two dimensionless differential equations [19]

$$i - i_{ni} = \beta_c \frac{d^2 \nu}{d\theta^2} + \frac{d\nu}{d\theta} + \sin \nu \cos \phi, \tag{2.32}$$

and

$$i_{ni} = \beta_c \frac{d^2 \phi}{d\theta^2} + \frac{d\phi}{d\theta} + \cos \nu \sin \phi + \frac{2}{\beta_L} (\phi - \phi_a), \tag{2.33}$$

where the beta parameter β_L is

$$\beta_L = \frac{2 I_c L}{\Phi_0}. \tag{2.34}$$

Equations (2.32) and (2.33) can be viewed as the equations of motion of the DC SQUID. According to numerical analysis of equations (2.32) and (2.33), in order to avoid magnetic hysteresis, the parameter β_L has to be less than one. Similarly, nonhysteretic current voltage characteristics require that $\beta_C \leq 1$.

Assuming that $C \approx 0$ and neglecting I_n, we can solve the voltage V from equations (2.27) and (2.28) as

$$
\begin{aligned}
V &= \frac{RI}{2}\left(1 - \frac{2I_c}{I}(\sin\gamma_1 + \sin\gamma_2)\right) \\
&= \frac{RI}{2}\left(1 - \frac{2I_c}{I}\cos\left(\frac{\pi\Phi}{\Phi_0}\right)\sin\left(\frac{\gamma_1 + \gamma_2}{2}\right)\right),
\end{aligned}
\tag{2.35}
$$

where we have substituted equation (2.19). The time averaged voltage is obtained by integrating equation (2.35) over the period of one Josephson oscillation, $T = \Phi_0/V$:

$$
\langle V \rangle = \frac{1}{T}\int_0^T V\, dt = \frac{RI}{2}\left(1 - \left(\frac{2I_c}{I}\cos\left(\frac{\pi\Phi}{\Phi_0}\right)\right)^2\right)^{1/2}.
\tag{2.36}
$$

For frequencies much less than the corresponding Josephson frequency, equation (2.36) effectively describes the DC current-voltage characteristics of the DC SQUID. Practical voltage bias points are larger than, say, 10 μV, so that the Josephson frequencies are > 4.8 GHz. Hereafter, we will assume that all operation frequencies are much less than the Josephson frequencies, and write the voltage across the SQUID as $V \equiv \langle V \rangle$.

The current-voltage characteristics are gathered into figure 2.3. Both current and voltage across the SQUID are periodic functions of flux with the period of one flux quantum. Equation (2.36) is valid only if the current I is greater than the critical current I_m from equation (2.26). If $I < I_m$, the SQUID is superconducting and equation (2.23) holds.

In practice, the SQUID is usually biased with DC current $I \simeq 2I_c$ across the SQUID, and constant applied flux $\Phi \simeq \Phi_0/4$ [7]. At the bias point, equation (2.36) reduces to

$$
V = \frac{RI}{2}\left(1 - \frac{2I_c^2}{I^2}\right)^{1/2},
\tag{2.37}
$$

from which, the effective resistance of the biased DC SQUID is

$$
R_d \equiv \left.\left|\frac{dV}{dI}\right|\right|_{\Phi=\Phi_0/4,\ I=2I_c} = \frac{R}{\sqrt{2}},
\tag{2.38}
$$

which is called the dynamic resistance.

2.4 Transfer Functions

Previously we showed that at the finite voltage region, the current, I, and the voltage, V, across the DC SQUID are periodic functions of flux enclosed by the
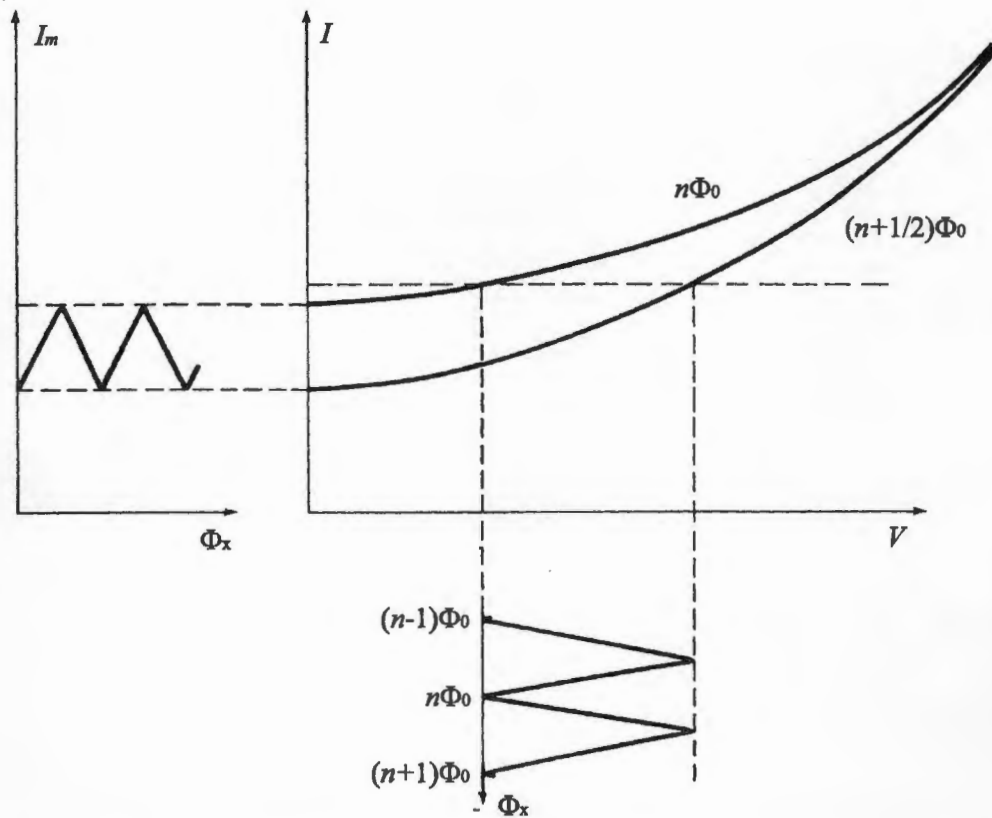
Figure 2.3: The IV characteristics of the DC SQUID. Both current and voltage are periodic functions of applied flux Φ_x with a period of Φ_0. The screening supercurrent rejects the 100% current-flux-modulation predicted by equation (7.1). Figure is obtained from ref. [4].

SQUID loop, Φ (equation (2.36)). A steep slope of current with respect to flux means that a small change in flux, $\delta\Phi \ll \Phi_0$, produces a large change in the current. A flux-to-current transfer function is defined as $I_\Phi = dI/d\Phi$. We can obtain an approximative result for I_Φ readily from the critical current formula (2.26):

$$I_\Phi = \frac{dI}{d\Phi} \approx 2I_c \frac{\pi}{\Phi_0} \sin\left(\frac{\pi\Phi}{\Phi_0}\right) = \frac{\beta_L \pi}{L} \sin\left(\frac{\pi\Phi}{\Phi_0}\right). \tag{2.39}$$

At the practical bias point, where $\Phi = \Phi_0/4$, the transfer function is

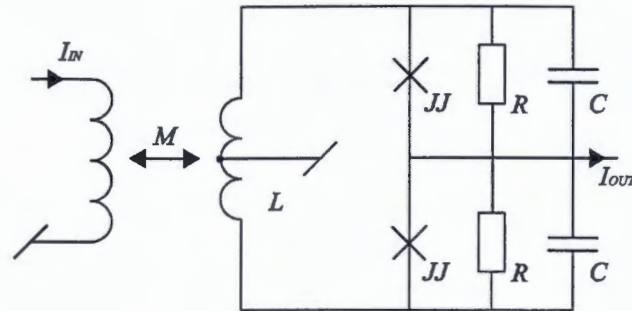$$I_\Phi \approx \frac{\beta_L \pi}{\sqrt{2}L}. \tag{2.40}$$

Figure 2.4: Simple equivalent circuit of the DC SQUID amplifier.

More exact derivation confirms that $I_\Phi = A/L$, where A is some constant in the order of unity. Correspondingly, the flux-to-voltage transfer function is defined as $V_\Phi = dV/d\Phi$. Using equation (2.40), the flux-to-voltage transfer function at the bias point is approximately

$$V_\Phi = \frac{dV}{d\Phi} \approx \frac{dV}{dI}\frac{dI}{d\Phi} \approx R_d\frac{\beta_L \pi}{\sqrt{2}L}. \tag{2.41}$$

The RCSJ-model of the DC SQUID amplifier is represented in figure 2.4.[5] The input coil inductance L_i is inductively coupled to the SQUID loop inductance L with coupling coefficient

$$\alpha^2 = \frac{M_i}{L_i L}. \tag{2.42}$$

where M is the mutual inductance between input coil and the SQUID loop. A current signal δI_{in} in the input coil induces a flux $\delta\Phi = M\delta I_{in}$. If the SQUID is properly biased, and the input signal amplitude is small, the transfer functions are nearly constant, and the output current is $\delta I_{out} = I_\Phi \delta\Phi = I_\Phi M \delta I_{in}$. Equivalently $\delta V_{out} = V_\Phi \delta\Phi = V_\Phi M \delta I_{in}$. Thus, the input signal is linearly amplified.

---

[5]The figure shows the typical construction where the two junctions are near each other, and most of the loop inductance is localized to the other electrode of the SQUID, the washer. Usually, the input coil and washer are grounded to reduce potential difference.

Chapter 3

LTL 800 SQUID Amplifier

LTL800 SQUID Amplifier was made in Technical Research Centre of Finland (VTT) from photolithographically patterned thin films of niobium with window type Josephson junctions.[1] The main designer was PhD Jari S. Penttilä from VTT Information Technology.

A picture of the complete LTL 800 circuit is shown in Figure 3.1. The corresponding simplified electrical circuit is also depicted. Here we will describe in separate sections the input coil and the SQUID (b), the input circuitry (a), and the output circuitry (c)-(e).

3.1 SQUID Design

LTL 800 is an advanced version of the typical DC SQUID construction first demonstrated by Jaycox and Ketchen [6]. Figure 3.2 shows the three successive niobium layers forming the SQUID and the input coil. The counter electrode at the first niobium layer (i), and the washer at the second niobium layer (ii) forms the body of the SQUID. The slit in the middle of the two layers determines the inductance of the SQUID. The two Josephson junctions (JJ) are near each other, and they are individually shunted by resistors (R) in order to damp hysteresis. The octagonal input coil is on the third niobium layer (iii). Most of the input coil is deposited over the superconductive washer, which works as a core of the coil collecting the induced magnetic flux into the slit, and consequently providing a good coupling between the input coil and the SQUID.

According to the Jaycox and Ketchen washer formula [12], the SQUID loop

---

[1]Several variations of LTL 800 SQUID Amplifier were fabricated. In this report, we will concentrate mainly on one type of the device.
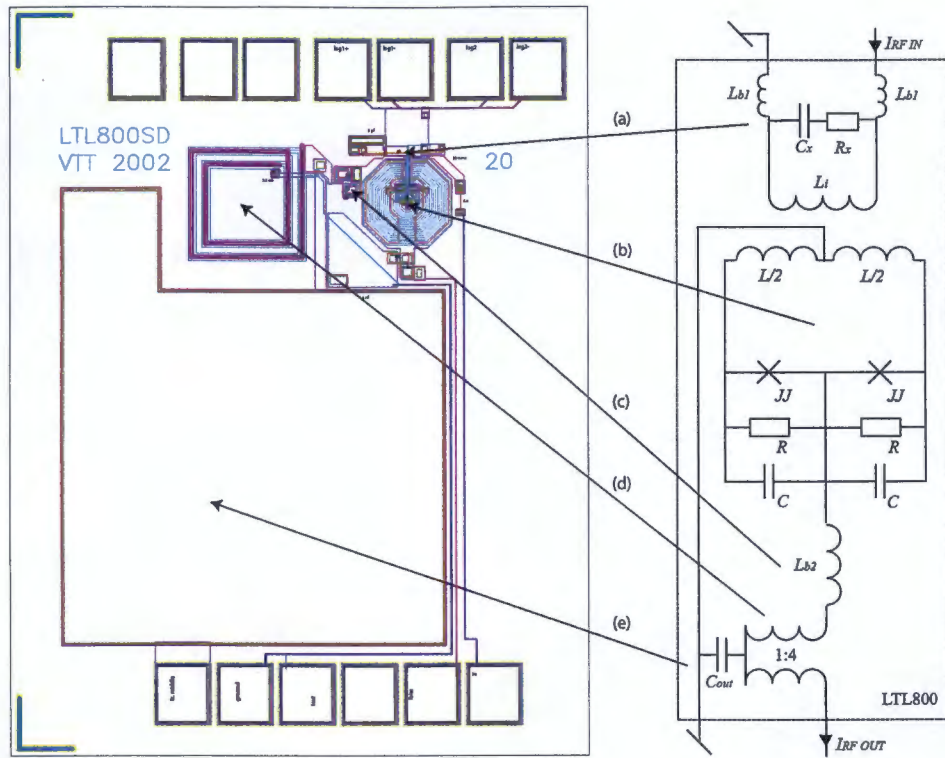
Figure 3.1: The LTL 800 CAD file showing the circuitry of the device. Size of the real chip is 1 mm x 2 mm. Corresponding equivalent circuit is also depicted, and the arrows shows the location of (a) the RC shunt, (b) the SQUID and the input coil, (c) the blocking inductor, (d) the output transformer, and (e) the output capacitor.
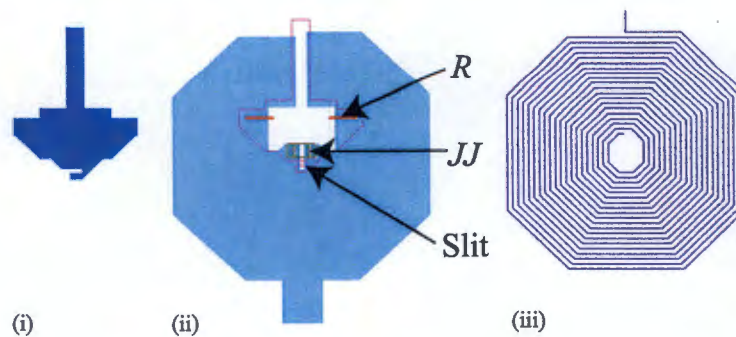

Figure 3.2: The three successive niobium layers forming (i) the counter electrode, (ii) the washer, and (iii) the input coil. The arrows points to the shunt resistor (R), the Josephson junction (JJ), and the slit.

inductance is

$$L = 1.25\mu_0 a, \tag{3.1}$$

requiring that the width of the washer is much larger than the side length a of the square slit. For LTL800, $a = 5$ μm, so that the loop inductance is predicted to be $L = 7.9$ pH. The other SQUID parameters were selected as follows: For optimal non-hysteretic operation, the beta parameters should be close to one. Choosing $\beta_L \approx 0.9$ required the junction critical current to be $I_c = \beta_L \Phi_0/2L = 120$ μA. The process yielded junction critical current density $J_c = 1200$ A/cm^2, which fixed the junction area to 1 μm^2, and the junction capacitance to $C = 300$ fF. To obtain $\beta_C \approx 0.9$, the shunt resistors became $R = (\beta_C \Phi_0/2\pi I_c C)^{1/2} \approx 2.7$ Ω.

The input coil consists of superconducting microstrips, width w, separated from the superconducting washer by insulator with dielectric constant ϵ and thickness d. If $w >> d$ and the superconducting penetration depth is less than the layer thickness, the inductance and capacitance per unit length are given by [12]

$$L_0 = \frac{\mu_0}{w}(d + 2\lambda) \tag{3.2}$$

and

$$C_0 = \frac{\epsilon\epsilon_0 w}{d}. \tag{3.3}$$

In our case, $w = 2$ μm, $d = 250$ nm, and $\epsilon = 4$, resulting $L_0 = 346$ nH/m and $C_0 = 283$ pF/m. [2] The characteristic microstrip impedance Z_0, and wave velocity c_0 are given by

$$Z_0 = \sqrt{\frac{L_0}{C_0}} = 35 \ \Omega, \tag{3.4}$$

and

$$c_0 = \frac{1}{\sqrt{L_0 C_0}} = 1.0 \cdot 10^8 \ \text{m/s}. \tag{3.5}$$

According the Jaycox and Ketchen model, the input coil inductance is

$$L_i = n^2 L + l_c L_0, \tag{3.6}$$

the mutual inductance is

$$M = nL, \tag{3.7}$$

and the coupling coefficient is

$$\alpha = \frac{M}{\sqrt{L_i L}}. \tag{3.8}$$

---

[2]The microstrip inductance and capacitance was also calculated as suggested by Chang [22], resulting $L_0 = 169$ nH/m and $C_0 = 410$ pF/m.

Here n is the number of turns of the input coil, and l_c is the length of the coil. For LTL 800, $n = 15$ and $l_c = 5.5$ mm, so that $L_i = 3.7$ nH, $M = 120$ pH and $\alpha = 0.70$. The total parasitic capacitance between the input coil and the SQUID washer is $C_p = l_c C_0 = 1.6$ pF.

The washer inductance and the junction capacitances give rise to the washer resonance. The presence of the input coil increases the capacitance across the loop by about $C_p/8$. The washer resonance is then at

$$f_w = \frac{1}{2\pi\sqrt{L(C + C_p/8)}} = 80 \text{ GHz.} \qquad (3.9)$$

3.2 Input Circuitry

The resonances in the input circuitry form resonant states for Josephson oscillations. Thermally activated transitions between different resonant states enhance the output noise. Additionally, the resonances cause disturbances on the average current-voltage characteristics.

The two lowest frequency resonances are the input circuit lumped resonance, and the microstrip resonance. The former determines the operation frequencies of the SQUID, and it will be studied extensively in the next chapter. For LTL 800, the lumped resonance is found around 650 MHz. The fundamental microstrip resonance occurs when the quarter wavelength[3] equals to the input coil length l_c:

$$f_m = \frac{c_0}{4l_c} = 4.6 \text{ GHz.} \qquad (3.10)$$

The input circuit lumped resonant states can be damped by terminating the input coil with a resistor-capacitor shunt. The RC-shunt lowers the Q-value of the input resonator circuit, which reduces the lifetime of the resonant state [19].

The quarter wave microstrip resonance disappears if the input coil is terminated with a resistor which is matched to the microstrip impedance [20]. The noise generated by the shunt resistor can be eliminated from signal frequencies using a RC-shunt instead of a pure resistor. At the microstrip resonance frequency, the impedance of the shunt capacitance must be small, but for optimum noise performance the capacitance should be minimized. Hence, the cutoff frequency of the capacitance should be somewhere around the microstrip resonance frequency.

Furthermore, the RC filter is an effective matching element, as will be shown in the next Chapter. In order to avoid reflections and to optimize noise perfor-

---

[3]If one end of the input coil is floating, instead of grounded as for LTL 800, the microstrip resonance occurs at half wavelength.

mance, the input impedance of any microwave amplifier should be matched to the signal source impedance.

The RC shunt for LTL 800 consists of a capacitance $C_s = 3\,\text{pF}$ and a resistance $R_x = 40\,\Omega$. The cutoff frequency for C_x is $f = (2\pi * C_x)^{-1} = 5.3\,\text{GHz}$. The Josephson oscillations are blocked by the $L_{b1} = 200\,\text{pH}$ inductances in the signal path.

3.3 Output Circuitry

The dynamic resistance determines the SQUID output impedance. The output transformer, pointed with the arrow (d) in figure 3.1, matches the SQUID output impedance, $R_d = R/\sqrt{2} \approx 1.9\,\Omega$, to the 50 Ω line. [4] In order to allow DC bias current and DC measurements, the output transformer is in series configuration, and the line connecting the primary and the secondary coils is connected to ground via the large capacitor (e) $C_{out} = 2.6\,\text{nF}$. The capacitor makes the coil functional above the frequency $f_{tr} = (2\pi C_{out})^{-1} = 61\,\text{MHz}$. Finally, the two coils (c) in figure 3.1 with total inductance $L_{b2} = 200\,\text{pH}$ blocks the Josephson oscillations from the output circuitry.

3.4 Concluding Remarks

There are three main characters that together make LTL 800 design potentially superior than the other SQUID amplifiers operating at microwave frequencies:

1. The lowest frequency resonant states for the Josephson oscillations are damped, which have been shown to improve the noise performance of the SQUID.

2. The SQUID loop inductance is small, which is supposed to result in a diminished intrinsic flux noise, and to allow a high frequency operation.

3. Both input and output is matched to 50 Ω impedance, making the amplifier convenient for various different applications.

---

[4]In principle, the transformer turns ratio should be $\sqrt{50/R_d} \simeq 5$, but numerical simulations required smaller ratio.

Chapter 4

Analytic Model

In this Chapter we will construct an analytic lumped element model for LTL 800 SQUID Amplifier. Particularly, the input impedance, gain, and noise performance will be studied. The model can be applied for estimating optimum parameter values for an RC-shunt tuned SQUID amplifier.

All given numerical results were obtained using the following approximative parameter values for LTL 800: the shunt resistance $R = 3\ \Omega$, SQUID loop inductance $L = 9$ pH, number of turns in the input coil $n = 15$, total input coil inductance $L_i = 5$ nH, and total parasitic capacitance between the input coil and the SQUID washer $C_p = 4$ pF.

4.1 Input Impedance

In this section we will derive a model for the input impedance of the RC-shunt tuned SQUID amplifier. In order to understand the effect of the RC-shunt, we will first consider a SQUID amplifier without any additional tuning elements.

4.1.1 Self-Resonant SQUID Amplifier

Since the input coil is tightly coupled to the SQUID loop, the simplest input model of a DC SQUID amplifier is a transformer shown in figure 4.1(a) [26]. The transforming ratio is $n^2 = L_i/\alpha^2 L$, where α is the coupling coefficient. As in any voltage transformer, the two junction resistances convert to an effective parallel resistance $R'_{sq} \equiv 2RL_i/\alpha^2 L$ resulting in the circuit in figure 4.1(b). The total impedance is then

$$Z_t = \left(\frac{1}{R'_{sq}} - j\frac{1}{\omega L_i} \right)^{-1} = \frac{\omega^2 L_i^2 R'_{sq} + j\omega L_i R'^2_{sq}}{R'^2_{sq} + \omega^2 L_i^2}. \qquad (4.1)$$
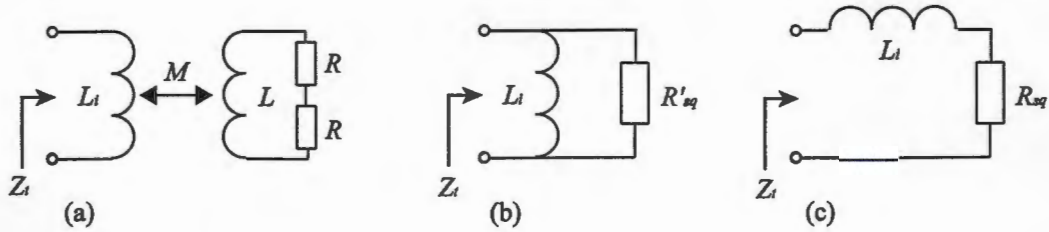
Figure 4.1: The impedance of the input coil and the SQUID. (a) The input coil is mutually coupled to the SQUID loop. (b) The SQUID impedance can be transformed to form an effective parallel resistance, R'_{sq}. (c) At the signal frequencies, the parallel circuit reduces to a series circuit consisting of input coil inductance and resistance R_{sq}.
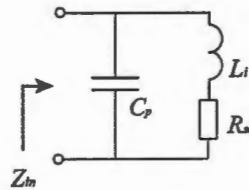

Figure 4.2: The input model for the self-resonant SQUID amplifier including the parasitic capacitance to the grounded washer.

Usually, the frequency

$$f = \frac{2R}{2\pi L} \tag{4.2}$$

is much larger than practical signal frequencies, so that

$$\omega L_i \ll R'_{sq}, \tag{4.3}$$

in which case equation (4.1) simplifies to

$$Z_t = \frac{\omega^2 M^2}{2R} + j\omega L_i \equiv R_{sq} + j\omega L_i, \tag{4.4}$$

where $M^2 = \alpha^2 L L_i$. Equation 4.4 corresponds to the circuit in figure 4.1(c).

Since the input coil is deposited above the grounded SQUID washer, there is significant distributed capacitance between input coil and ground. The simplest approximation for such a device is depicted in figure 4.2, for which the input impedance is

$$
\begin{aligned}
Z_{in} &= \left[j\omega C_p + (j\omega L_i + R_{sq})^{-1} \right]^{-1} \\
&= \left[\frac{R_{sq}}{R_{sq}^2 + \omega^2 L_i^2} + j\left(\omega C_p - \frac{\omega L_i}{R_{sq}^2 + \omega^2 L_i^2} \right) \right]^{-1}.
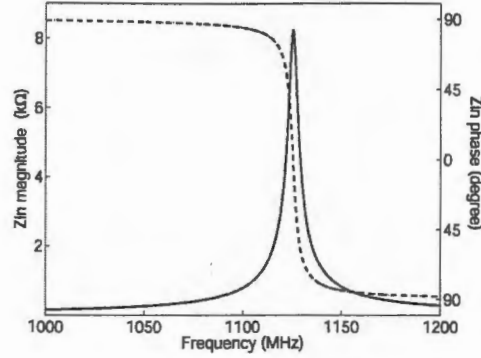\end{aligned} \tag{4.5}
$$

Figure 4.3: Magnitude (solid curve) and phase (dashed curve) of the input impedance for the self-tuned SQUID amplifier.

Since $R_{sq} \ll \omega L_i$, equation (4.5) reduces to

$$Z_{in} = \left[\frac{M^2}{2RL_i^2} + j \left(\omega C_p - \frac{1}{\omega L_i} \right) \right]^{-1}, \tag{4.6}$$

from which the parallel resonance frequency is

$$f_0 = \frac{1}{2\pi \sqrt{C_p L_i}} \approx 1.1 \text{ GHz}, \tag{4.7}$$

where we have substituted the parameter values given at the beginning of the chapter. At the resonance, the imaginary part is zero, and the real part is evidently

$$Z_{in} = \frac{2RL_i^2}{M^2} \approx 8.2 \text{ k}\Omega. \tag{4.8}$$

The quality factor of the parallel resonator is

$$Q = \frac{Z_{in}(\omega_0)}{\omega_0 L_i} = \frac{2RL_i}{\omega_0 M^2} = \frac{2RL_i \sqrt{L_i C_p}}{M^2} \approx 233, \tag{4.9}$$

and the bandwidth is

$$\text{BW} = \frac{f_0}{Q} = \frac{\omega_0^2 M^2}{4\pi R L_i} = \frac{M^2}{4\pi R C_p L_i^2} \approx 4.8 \text{ MHz}. \tag{4.10}$$

The magnitude and phase of the input impedance is plotted from equation (4.5) in figure 4.3(a). The input impedance is almost purely imaginary everywhere but at the narrow bandwidth resonance. Such an input impedance is unsuitable for a microwave amplifier, since it will reflect effectively all incident signal. We
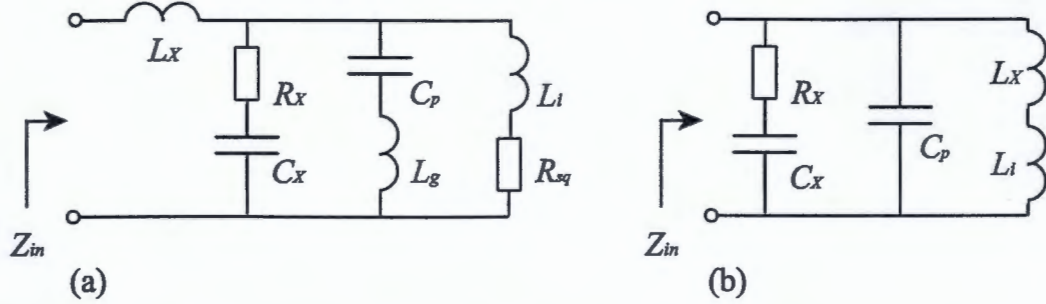
Figure 4.4: (a) The model of the LTL 800 input circuitry taking into account the RC-shunt terminating the input coil, the stray inductance L_x, and the inductance in ground, L_g. (b) The simplified model, where the stray inductances are approximated by inductance, $L_i' \approx L_x + L_i$.

can show this by considering the voltage reflection coefficient, $|\Gamma_{in}|$, for a source signal with characteristic impedance Z_0:[1]

$$\Gamma_{in}(\omega) = \frac{Z_{in}(\omega) - Z_0}{Z_{in}(\omega) + Z_0}. \tag{4.11}$$

Separating the real and imaginary part of the input impedance and assuming $\Im\{Z_{in}\} \gg \Re\{Z_{in}\} \approx 0$, we can write

$$|\Gamma_{in}|^2 \approx \left| \frac{j\Im\{Z_{in}\} - Z_0}{j\Im\{Z_{in}\} + Z_0} \right|^2 = \frac{\Im\{Z_{in}\}^2 + Z_0^2}{\Im\{Z_{in}\}^2 + Z_0^2} = 1. \tag{4.12}$$

Consequently, in order to avoid reflections, the input impedance of a microwave SQUID amplifier must be tuned, i.e. matched to the source signal impedance.

4.1.2 LTL 800 SQUID Amplifier

The RC-shunt terminating the input coil has a prominent effect on the input impedance of LTL 800 SQUID amplifier. Figure 4.4(a) presents a lumped element model for LTL800 input circuitry. The resistance R_x, and capacitance C_x form the RC-shunt. The inductance L_x corresponds to the stray inductance in the signal bath, and the inductance L_g presents the stray inductance found in the ground connection between the SQUID washer and the grounded end of the input coil. The inductances L_x and L_g are estimated to be 3 nH and 6 nH, respectively.

---

[1]For simplicity, we assume that the signal source is impedance is real and equals to the characteristic impedance of the feed line.

The input impedance for the model is

$$Z_{in} = j\omega L_x + \left[\left(R_x - \frac{j}{\omega C_x} \right)^{-1} + \left(j\omega L_g - \frac{j}{\omega C_p} \right)^{-1} \right.$$
$$\left. + \left(j\omega L_i + \frac{\omega^2 M^2}{2R} \right)^{-1} \right]^{-1}. \tag{4.13}$$

Equation (4.13) is plotted in figure 4.5(a). Corresponding measured plot of the LTL 800 input impedance is shown in figure 4.5(b). Considering the simplicity of the model, the similarity of the two plots is remarkable. According to the model, the path through L_x, C_p, and L_g forms a series resonator causing the conductance peak at 920 MHz. At the series resonance, the input coil is, effectively, shunted by the parasitic capacitance.

The magnitude of the input impedance at the resonance is determined by the RC-shunt, instead of the transformed SQUID impedance, which is why the impedance is much lower than in the case of the self-tuned amplifier (figure 4.3). This can be shown analytically, if we simplify the input model further by replacing the three inductances L_i, L_g, and L_x by an enlarged input coil inductance $L_i' \approx L_i + L_x = 8$ nH, as depicted in figure 4.4(c). The simplified input impedance is

$$Z_{in} = \left[\left(R_x - \frac{j}{\omega C_x} \right)^{-1} + j\omega C_p - \frac{j}{\omega(L_i + L_x)} \right]^{-1}$$
$$= \left[\frac{R_x}{R_x^2 + (\omega C_x)^{-2}} + j\left(\omega C_p - \frac{1}{\omega(L_i + L_x)} + \frac{1}{\omega C_x R_x^2 + (\omega C_x)^{-1}} \right) \right]^{-1} \tag{4.14}$$

The simplified model predicts the parallel resonance correctly as seen from figure 4.5(c). The resonance frequency can be solved, if we approximate that $(\omega C_x)^{-1} \gg \omega C_x R_x^2 \approx 0$. The result is

$$f_0 = \frac{1}{2\pi\sqrt{(C_p + C_x)(L_i + L_x)}} \approx 673 \text{ MHz}, \tag{4.15}$$

which is approximately equal to the resonance frequency 670 MHz obtained numerically from equation (4.14) or (4.13). According to the Jaycox and Ketchen model described in Chapter 3, the input coil inductance is $L_i \simeq n^2 L + L_m$, where $L_m \approx 2$ nH is the total microstrip inductance. Thus increasing the SQUID loop inductance L, or the number of turns n, limits the operation frequencies. At the resonance, equation (4.14) reduces to

$$Z_{in}(\omega_0) = R_x + \frac{1}{\omega_0^2 C_x^2 R_x} \approx 196.7 \ \Omega, \tag{4.16}$$
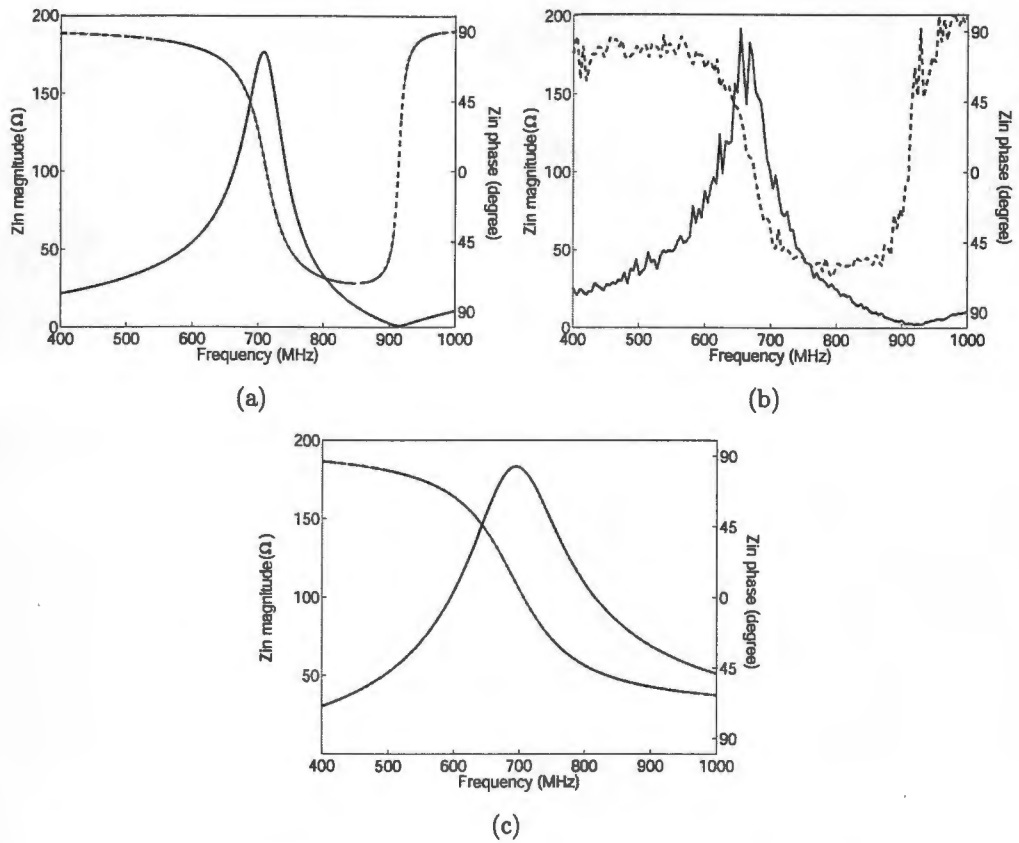
(a)

(b)

(c)

Figure 4.5: Magnitude (solid line) and phase (dashed line) of the input impedance of LTL 800 with 15 turn input coil obtained (a) from the circuit in figure 4.4(b), (b) experimentally, and (c) from the simplified circuit in figure 4.4(c).
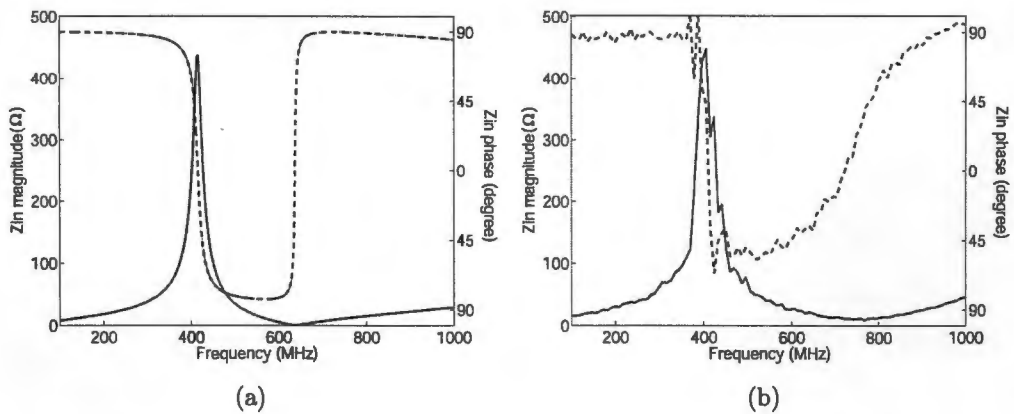

(a)

(b)

Figure 4.6: (a) Simulated, and (b) measured magnitude (solid line) and phase (dashed line) of the input impedance of LTL 800 with 20 turn input coil.

where we have used the measured value $f_0 = 670$ MHz. Substituting equation (4.15) leads to

$$Z_{in}(\omega_0) = R_x + \frac{(C_p + C_x)(L_i + L_x)}{C_x^2 R_x} \approx 195.6 \ \Omega. \tag{4.17}$$

Equations (4.16) and (4.17) confirm that the RC-shunt has the main contribution to the impedance at the resonance, as stated. The quality factor for the simplified model is

$$Q = \frac{Z_{in}(\omega_0)}{\omega_0(L_i + L_x)} = \frac{\omega_0^2 R_x^2 C_x^2 + 1}{\omega_0^3(L_i + L_x)R_x C_x^2} \approx 5.8. \tag{4.18}$$

and the corresponding bandwidth is

$$\text{BW} = \frac{f_0}{Q} = \frac{1}{2\pi} \frac{\omega_0^4(L_i + L_x)R_x C_x^2}{\omega_0^2 R_x^2 C_x^2 + 1} \approx 115 \ \text{MHz}. \tag{4.19}$$

Thus, the RC-shunt lowers the quality factor and increases the bandwidth.

As indicated in the footnote in Chapter 3, there is several variants of LTL 800 SQUID Amplifier. To check the performance of the model, let us now consider LTL 800 with 20 turns input coil. The ratio of the lengths of the 20 and 15 turns coils is 9/5.5=1.64, so that the parasitic capacitance C_p and input coil inductance L_i of the 20 turn input coil can be predicted to be approximately 1.64 times larger. The parallel resonance frequency corresponds to the measured one if the coefficient is 2, i.e. $L_i = 10$ nH and $C_p = 8$ pF. Using these values, we obtain the frequency response of the input impedance shown in figure 4.6(a), which corresponds well to the measured input impedance is shown in figure 4.6(b). Equations (4.16) and (4.17) give $Z_{in}(\omega_0 = 416 \text{ MHz}) = 447 \ \Omega$, $Z_{in}(\omega_0) = 437 \ \Omega$, and $f_0 = 421$ MHz, respectively, which confirms that also the approximate formulas seem to work properly.

As argued in Chapter 3, the RC-shunt improves the SQUID amplifier performance in various ways, and therefore the values of R_x and C_x are not determined exclusive by the impedance matching. Accordingly, some additional matching method may be needed in order to completely match the input impedance, for example, to a 50 Ω line.

4.2   Forward Gain

The scattering parameters S_{ik} are defined as the complex (amplitude and phase) ratio of the voltage signal V_k^- leaving the test device port k, to the signal V_i^+ entering to the test device port i:

$$S_{ik} = \frac{V_i^-}{V_k^+}. \tag{4.20}$$

For LTL 800, the dynamic impedance of the SQUID is matched to $Z_0 = 50$ Ω, in which case $V_2^+ = 0$, and the reflection coefficient S_{11} is[2] [5]

$$S_{11} = \frac{V_1^-}{V_1^+} = \Gamma_{in} = \frac{Z_{in} - Z_0}{Z_{in} + Z_0}, \tag{4.21}$$

where Z_{in} is the input impedance of the test device. The voltage signal delivered to the SQUID input is then $V_{in} = V_1^+(1 - \Gamma_{in})$, which generates current $I_i = V_{in}/Z_t$ in the input coil, where $Z_t = R_{sq} + j\omega L_i$ is the input transformer impedance (equation (4.4)). The current I_i gives rise to an output voltage $V_{out} = V_\Phi M I_i$, where V_Φ is the flux-to-voltage transfer function (equation (2.41)). The output transformer matches the SQUID dynamic resistance R_d to Z_0, so that, for an ideal transformer, the transforming ratio would be $n_o = \sqrt{Z_0/R_d}$. The voltage leaving the LTL 800 output port is then

$$\begin{aligned}
V_2^- &= V_{out} n_o \\
&= \frac{V_\Phi M V_{in}}{Z_t} n_o \\
&= \frac{V_\Phi M V_1^+}{Z_t}(1 - \Gamma_{in}) n_o.
\end{aligned} \tag{4.22}$$

The forward gain of the two port network is then

$$S_{21} = \frac{V_2^-}{V_1^+} = \frac{V_\Phi M}{Z_t}(1 - \Gamma_{in}) n_o, \tag{4.23}$$

which corresponds to the "forward" power gain

$$G = \frac{|V_2^-|^2/(2Z_0)}{|V_1^+|^2/(2Z_0)} = \frac{|V_\Phi M|^2}{|R_{sq} + j\omega L_i|^2}\left(1 - |\Gamma_{in}|^2\right) n_o^2. \tag{4.24}$$

At the signal frequencies, $\omega L_i \gg R_{sq}$, and we can neglect R_{sq} from equation (4.24). Substituting $n_o = \sqrt{Z_0/R_d}$, $M = nL$ and $|V_\Phi| = AR_d/L$, where A is a constant order of unity (see equation (2.40)), we attain

$$G(\omega) = A^2 \frac{n^2 Z_0 R_d}{\omega^2 L_i^2}\left(1 - |\Gamma_{in}(\omega)|^2\right). \tag{4.25}$$

As shown in previous section, if $\Re(Z_{in}) \ll \Im(Z_{in})$ the magnitude of reflection coefficient is unity, and $(1 - |\Gamma_{in}|^2) \approx 0$. Therefore, the operation frequencies are determined by the input circuit parallel resonance and the corresponding bandwidth.

---

[2]Here we assume that there is no feedback, i.e. that the amplified signal does not couple back to the input.
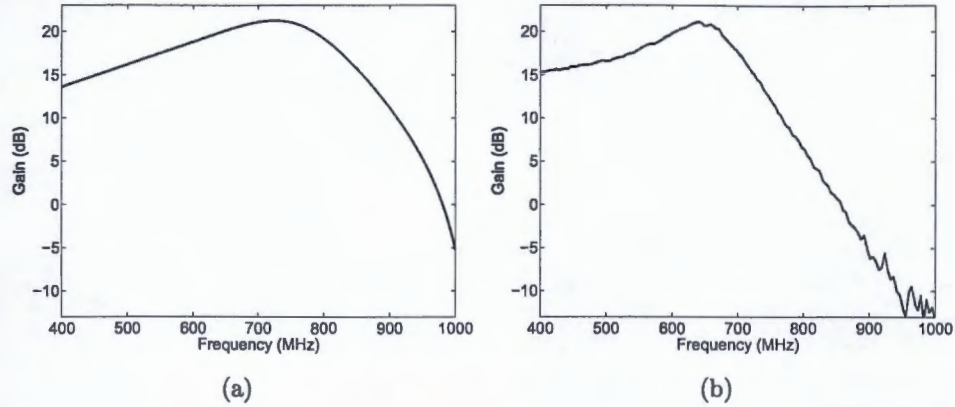
Figure 4.7: (a) The simulated, and (b) measured frequency response for the power gain of LTL 800.

Figure 4.7(a) shows the frequency response of the power gain obtained from equations (4.25) and (4.13). Again, the model manages to explain the behavior of the measured data shown in figure 4.7(b).

The power gain has a maximum near the resonance frequency $\omega = \omega_0$. Substituting the approximate formula for ω_0, equation (4.15), into equation (4.25) leads to

$$G(\omega_0) = AZ_0 R_d n^2 \frac{(L_i + L_x)(C_p + C_x)}{L_i^2} \left(1 - |\Gamma_{in}(\omega_0)|^2\right) \approx 21.4 \text{ dB}, \qquad (4.26)$$

where we substituted $A = 2$, and the reflection coefficient was calculated from (4.21) using $Z_{in}(\omega_0) = 196 \ \Omega$. Approximating $L_i \gg L_x \approx 0$, and inserting $L_i = n^2 L + L_m$, we can write equation (4.26) as

$$G(\omega_0) = AZ_0 R_d \frac{C_p + C_x}{L + L_m/n^2} \left(1 - |\Gamma_{in}(\omega_0)|^2\right) \approx 20.3 \text{ dB}, \qquad (4.27)$$

In order to maximize the gain one should maximize the shunt resistances R. However as indicated in Chapter 2, the SQUID operation may be hysteretic, if the beta parameters, equation (2.31)

$$\beta_C = \frac{2\pi I_c R^2 C}{\Phi_0}, \qquad (4.28)$$

and equation (2.34)

$$\beta_L = \frac{2 I_c L}{\Phi_0}, \qquad (4.29)$$

are greater than one. Eliminating I_c from equations (4.28) and (4.29), we get

$$R^2 = \frac{\beta_C}{\beta_L} \frac{L}{\pi C}. \qquad (4.30)$$

Thus, larger SQUID loop inductance allows greater shunt resistors.

4.3   Noise Performance

The spectral noise density generated by the shunt resistor R at temperature T can be described by a series voltage noise source $v_n = \sqrt{4k_BTR}$, or with a parallel current noise source $i_n = \sqrt{4k_BT/R}$. The corresponding voltage and current noise are $\langle V_n^2 \rangle^{1/2} = v_n\sqrt{\Delta f}$, and $\langle I_n^2 \rangle^{1/2} = i_n\sqrt{\Delta f}$, where Δf is the bandwidth.

The two shunt resistors generate noise voltage $\sqrt{4k_BT(R/2)} = v_n/\sqrt{2}$ across the SQUID, and circulating noise current $\sqrt{4k_BT/(2R)} = i_n/\sqrt{2}$ in the SQUID loop[3]. The circulating current induces voltage

$$v_{n,i} = \frac{M}{\sqrt{2}}\frac{di_n}{dt} = -i\omega\frac{M}{\sqrt{2}}i_n \tag{4.31}$$

in the input coil. The induced voltage produces a noise current

$$i_{n,i} = \frac{v_{n,i}}{Z_t}, \tag{4.32}$$

in the input coil, where Z_t is the input transformer impedance (4.4). Also, the RC-shunt (see figure 4.4) generates noise current into the input coil. The RC-shunt is a high pass filter with a standard transfer function

$$F(\omega) = \frac{i\omega R_x C_x}{i\omega R_x C_x + 1}. \tag{4.33}$$

The attenuated squared current noise at the input coil is then

$$i_{n,x}^2 = \frac{v_{n,x}^2}{|Z_t|^2}|F|^2, \tag{4.34}$$

where $v_{n,x} = \sqrt{4k_BTR_x}$. The noise current in the input coil transfers to the SQUID output producing output voltage

$$v_{n,o}^2 = (MV_\Phi)^2 \left(i_{n,i}^2 + i_{n,x}^2 \right). \tag{4.35}$$

The total spectral density of voltage noise $v_{n,tot}$ at the SQUID output is

$$v_{n,tot}^2 = \frac{v_n^2}{2} + \frac{v_{n,o}^2}{2} = \frac{v_n^2}{2} + \frac{\omega^2 M^4 V_\Phi^2}{|Z_t|^2}\frac{i_n^2}{2} + \frac{M^2 V_\Phi^2 |F|^2}{|Z_t|^2}v_{n,x}^2. \tag{4.36}$$

The corresponding spectral density of voltage noise at SQUID output is

$$S_v(\omega) = 4k_BT \left(\frac{R\gamma_v}{2} + \frac{\omega^2 M^4 V_\Phi^2}{|Z_t|^2}\frac{\gamma_i}{2R} + \frac{M^2 V_\Phi^2 |F|^2}{|Z_t|^2}R_x\gamma_x. \right) \tag{4.37}$$

---

[3]For the DC SQUID, the voltage and current noise generators are not independent, since the circulating noise current effects on the voltage across the junctions and vice versa. However, at low bias currents, the cross correlations can be neglected [20].
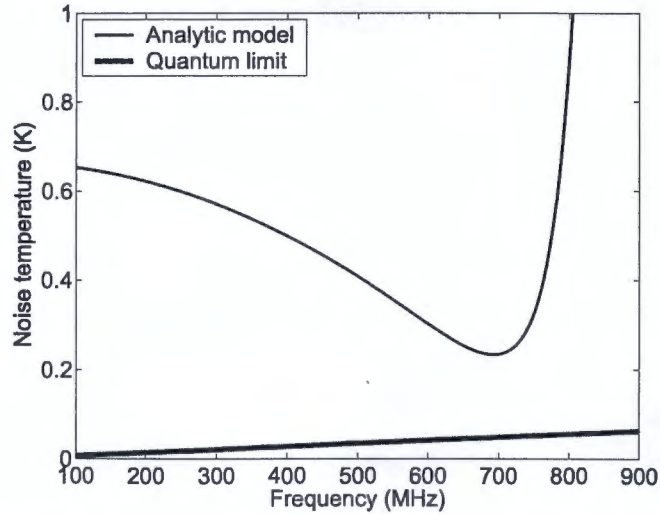
Figure 4.8: The classical noise temperature at 4 K bath temperature as a function of frequency, and the quantum limit for minimum noise temperature.

where γ_v, γ_i, and γ_d are the noise spectral coefficients of the different noise sources. Particularly, the coefficients should take into account the cross-correlation between the voltage and current noise sources [23, 24], and the mixing-down of the high frequency noise from Josephson oscillation, shunt resistors, and RC-shunt [20]. Calculating the coefficients is beyond the scope of this Thesis.

The noise temperature referred to the signal source impedance Z_0 is

$$T_n = \frac{S_v(\omega)}{4k_B R_i G(\omega)}, \tag{4.38}$$

where G is the power gain from equation (4.25). According to equations (4.37) and (4.38), the SQUID amplifier noise temperature depends linearly on the bath temperature T, which is quite obvious, if the noise originates entirely from the resistances. The bias current heats the shunt resistances limiting the minimum attainable resistor temperature, and thus the minimum noise temperature.

The frequency dependence of the noise temperature at $T = 4.2$ K obtained from equations (4.37) and (4.38) using typical values $\gamma_i = \gamma_v = \gamma_d = 5$, and $Z_0 = 50\,\Omega$, is shown in figure 4.8. This simple model predicts an extremely low noise temperature, as low as 300 mK at liquid helium temperatures. We want to emphasize that the simple model given here is only for qualitative purposes. In a real SQUID, the values of γ_i and γ_v may be 2-5 times larger [18].

Koch, Van Harlingen, and Clarke [16] studied the zero point fluctuations in the shunt resistances, and they found that the noise temperature for an optimized

system at $T = 0$ K is

$$T_n \approx \frac{hf}{k_B \ln 2}. \tag{4.39}$$

The quantum limit is included in figure 4.8. For 700 MHz signal frequency, the optimum noise temperature is 49 mK. According to the simple model, the quantum limited operation could be achieved by cooling our SQUID amplifier to 700 mK.

Chapter 5

Computer Simulation Model

A commercial circuit simulation software by Aplac Solutions Corporation has been exploited in several phases of the amplifier project. Initially, Jari S. Penttilä wrote a circuit model for the designing process. In this work, the model has been improved in order to explain the experimental results.

5.1 Input Model

The input model simulates the combined system of the input coil and the SQUID. Figure 5.1(a) shows the circuit model of the input transformer. Each input coil turn is inductively and capacitively coupled to the SQUID washer. Additionally, the input coil loops are inductively coupled to each other. Parasitic capacitances between adjacent turns are also taken into account.

The mutual inductance for single turn is approximately equal to the SQUID loop inductance: $M_{wm} \simeq L$. As described in Chapter 2, a small change in the current I_m in a single turn of the input coil causes a change in flux $\delta\Phi = M_{wm}\delta I_m = L\delta I_m$, which then changes the output current as

$$\delta I_{out,m} = I_\Phi \delta\Phi = \frac{A}{L}L\delta I_{in} = AI_{in}. \tag{5.1}$$

Thus, the properly biased DC SQUID can be viewed as a current controlled current source, as depicted schematically in figure 5.1(b). The input model calculates current in each loop, $I_1, I_2, ..., I_n$, and produces an output current

$$I_{out} = A\sum_{m=1}^{n} I_{out,m}. \tag{5.2}$$

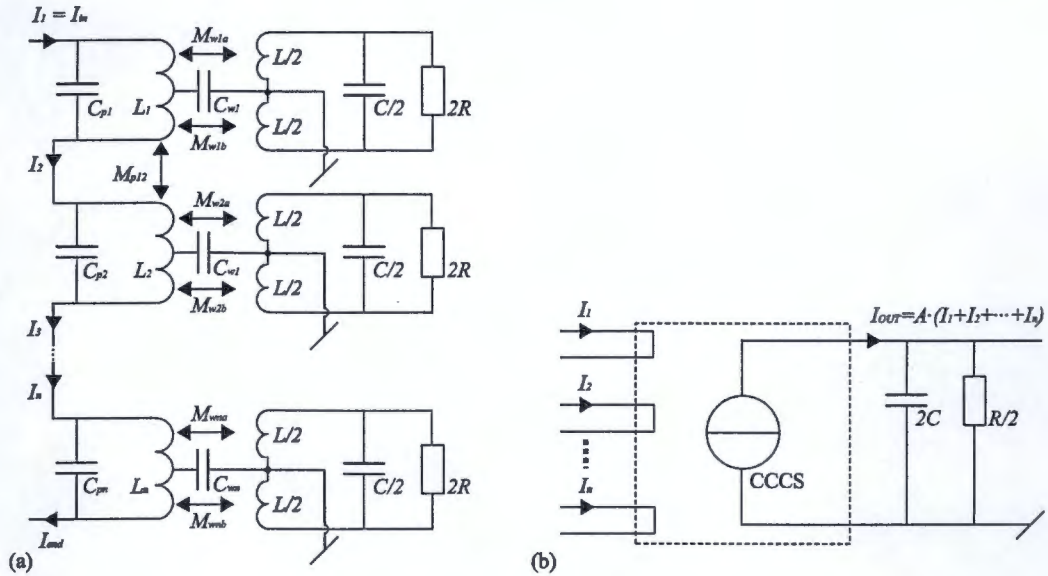According to Chapter 2, the constant A is approximately unity.

Figure 5.1: The model of the input coil and the SQUID (a) towards input, and (b) towards output. The SQUID is effectively an input coil Current Controlled Current Source.

The input coil inductance is calculated separately for each loop using the Jaycox and Ketchen model described in Chapter 3. The inductance of the innermost loop is

$$L_1 = L + L_0 l_1. \tag{5.3}$$

The length of the first loop is $l_1 \approx 95 \ \mu\text{m}$, the measured value of the SQUID loop inductance is $L = 8.6$ pH, and in Chapter 3 we obtained for the microstrip inductance $L_0 \simeq 350 \ \text{nH/m}$, so that $L_1 \approx 33$ pH. The length of each turn increases with a constant increment $\delta l = 39 \ \mu\text{m}$ per turn. The inductance of the m:th loop is then

$$L_m = L + L_0(l_1 + (m-1)\delta l). \tag{5.4}$$

The microstrip capacitance per unit length is $C_0 = 410$ pF/m, so that the microstrip capacitance for the innermost loop is $C_1 = C_0 l_1 = 39$ fF, and of the m:th loop

$$C_m = C_0(l_1 + (m-1)\delta l). \tag{5.5}$$

The capacitance between the two smallest loops was estimated to be around 10 fF.

In the model, the SQUID loop inductance is divided into two equivalent parts $L_a = L/2$ and $L_b = L/2$ (see figure 5.1). The coupling coefficients between
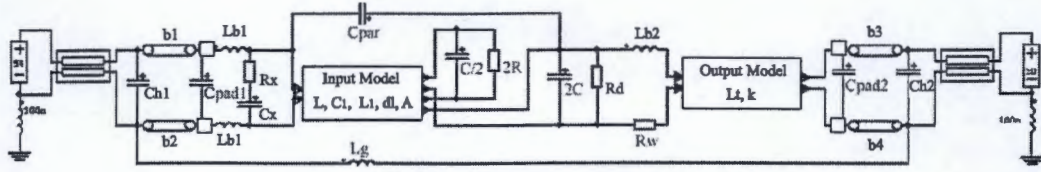
Figure 5.2: The Aplac circuit simulation model of LTL 800. The model corresponds to the network analyzer measurement.

washer and input coil turn m, is calculated separately for both parts:

$$\alpha_{am} = \alpha_{bm} = \frac{L/2}{\sqrt{L_m L/2}}. \tag{5.6}$$

The coupling coefficients between parallel input coil turns l and m is found from

$$\alpha_{lm} = \frac{L}{\sqrt{L_l L_m}}. \tag{5.7}$$

5.2 Output model

The output model simulates the 1:4 output transformer. The two primary turns and eight secondary turns are in the successive niobium layers. The inductance and the parasitic capacitance for each secondary coil turn, is calculated using formulas equivalent to (5.4) and (5.5). The coupling coefficients between the primary and secondary coil turns, and the coupling coefficients between the parallel secondary coil turns are then attained from the common formulas, such as equation (5.7). Both coils are connected to ground through the same 2.6 nF capacitor.

5.3 Full Model

The full model is shown in figure 5.2. To reduce unnecessary complexity, we have excluded all components which, with realistic parameter values, we have found to be insignificant. The model in the figure simulates network analyzer measurement. The outermost components of the model are the two 50 Ω ports of the network analyzer. The four squares in the figure shows the location of the aluminum pads on the SQUID chip. The transmission lines simulates the striplines and connectors in the sample holder. The parallel capacitances C_{h1} and C_{h2} corresponds to the capacitance in the sample holder, while C_{pad1} C_{pad2} corresponds to the capacitance in the pads and microstrips.

Table 5.1: The estimated minimum and maximum values, and fitted values for the main parameters in the Aplac model.

Variable	Description	Estimated	Fitted	Unit
R	SQUID shunt resistance	2.7 ± 0.1	2.7	Ω
R_d	SQUID dynamic resistance	1.9 ± 0.5	2.4	Ω
C	SQUID shunt capacitance	300 ± 100	300	fF
R_x	RC-shunt resistor	40 ± 2	40	Ω
C_x	RC-shunt capacitor	3 ± 0.1	3	pF
L_{b1}	Blocking inductance	200 ± 100	200	pH
L_{b2}	Blocking inductance	200 ± 50	150	pH
R_w	Washer resistance	0.5 ± 0.1	0.1	Ω
C_{par}	Parasitic capacitance	100 ± 50	700	pF
L_g	Ground connection inductance	4 ± 2	5	nH
C_{pad1}	Pad capacitance	70 ± 50	100	fF
C_{pad2}	Pad capacitance	700 ± 300	200	fF
C_{x1}	Holder capacitance	70 ± 60	100	fF
C_{x2}	Holder capacitance	70 ± 40	100	fF
$b1$	Bond wire length	0.7 ± 0.3	0.5	mm
$b2$	Bond wire length	0.7 ± 0.3	0.5	mm
$b3$	Bond wire length	1 ± 0.5	1	mm
$b4$	Bond wire length	1 ± 0.5	1	mm
A	Transfer function coefficient	1 ± 1	1	
C_1	The innermost input loop microstrip cap.	39 ± 20	80	fF
L_1	The innermost input loop microstrip ind.	33 ± 10	25	pH
δl	Input coil length increase per turn	39 ± 2	39	μm
L_t	Output coils loop inductance per turn	600 ± 100	800	pH
k	Coupling between prim. output coil turns	0.8 ± 0.1	0.6	

Aluminum bond wires connect the sample holder to the pads. The wire model takes into account the distributed inductance (about 1 nH/mm), capacitance, and resistance, as well as the phase delay. The bond wires at the SQUID output are somewhat enlarged to include the inductance in the output microstrip.

The input and output circuitry are not connected on the SQUID chip, but in the experimental setup, the input coil and the SQUID washer are both grounded via the bond wires, and thus they are connected through a copper stripline on the sample holder. The inductance L_g in the ground connection stripline on our sample holder is estimated to be about 5 nH.

The capacitance C_{par} simulates the parasitic capacitance between the input coil and the counter electrode. If C_{par} is large, a part of the amplified signal may couple back to the input coil resulting feedback. Our calculations estimates $C_{par} \approx 100$ pF, but fitting to the experimental data requires 700 pF capacitance, which is the only clearly unrealistic parameter value in the model.

The main parameters are gathered into table 5.1. The table gives both, the estimated parameter values, and the values that provides the best fit to the measured data. The simulation results presented in Chapter 7 are obtained using these values.

Chapter 6

Experimental Configurations

LTL 800 SQUID Amplifier was characterized experimentally liquid ^{4}He bath using a dip stick cryostat. Two 50 Ω coaxial cables with copper inner wire, copper coating, teflon dielectric, and SMA-connectors for microwave signals, and eight twisted pairs for DC wiring, were installed into the stick. A sample holder was carefully designed to minimize reflections and resonances. We installed aluminum wires between the sample and holder with a Delvotec bonder. HP 33120A Function Generators produced bias currents via applying voltage over 10 kΩ resistors. Measurement electronics were connected to a computer through GPIB ports, and Matlab software with Control-toolbox was used for automatized instrument control and data collection.

The DC SQUID is extremely sensitive magnetometer, and thus easily disturbed by electromagnetic noise. To avoid the 50 Hz noise in bias currents, a self-made optical isolation box separated the function generator ground from the measurement ground. A cryoperm μ-metal can with lead foil inside acted as a shield for radiation and magnetic noise.

6.1 Direct Current Measurement

The DC current-voltage measurement setup is depicted in figure 6.1. A Stanford Research Systems SR560 preamplifier amplified the voltage across the SQUID. The function generators swept the voltage across the 10 kΩ resistors with a frequency of 7 Hz, and an accurate high speed data logger, National Instruments PCI-6115 Multifunction Data Acquisition devise (DAQ), monitored simultaneously the bias voltages and the amplified voltage across the SQUID.
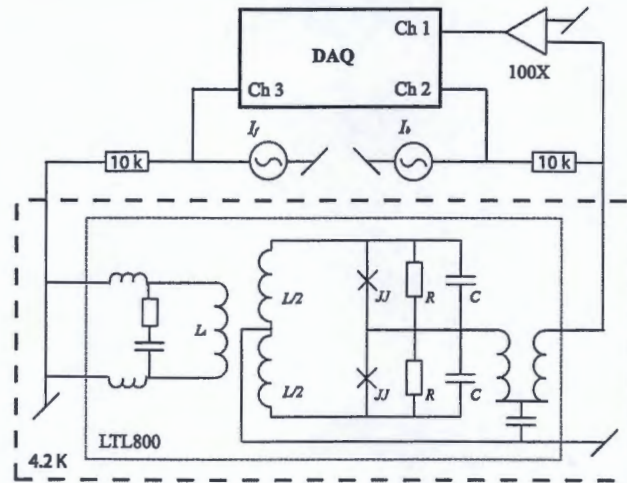
Figure 6.1: The DC measurement schematics. Data acquisition devise (DAQ) monitored simultaneously the bias voltages.
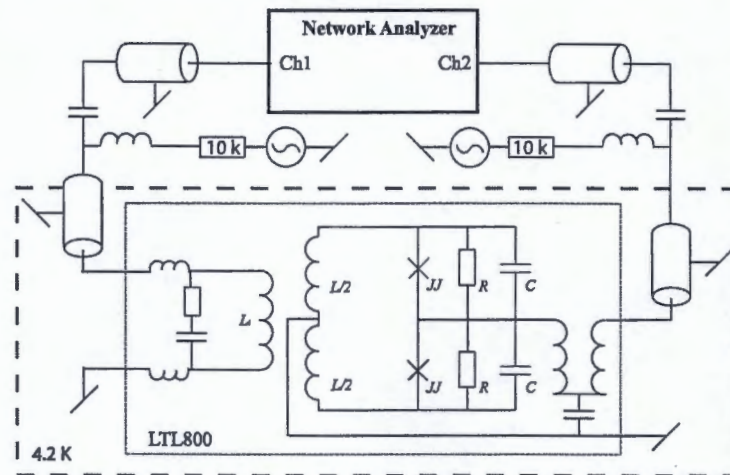

Figure 6.2: The setup in the scattering parameter measurements.

6.2 Network Characterization Setup

The setup for two port microwave network characterization with a Hewlett Packard 8753E vector network analyzer is shown schematically in Figure 6.2. Mini-Circuit ZFBT-4R2GW bias-T components combined the DC bias current and the microwave signal into the same coaxial line, and allowed a simultaneous DC measurement. The DC measurement setup was identical to the one described in previous section, and for simplicity it is not included in Figure 6.2.
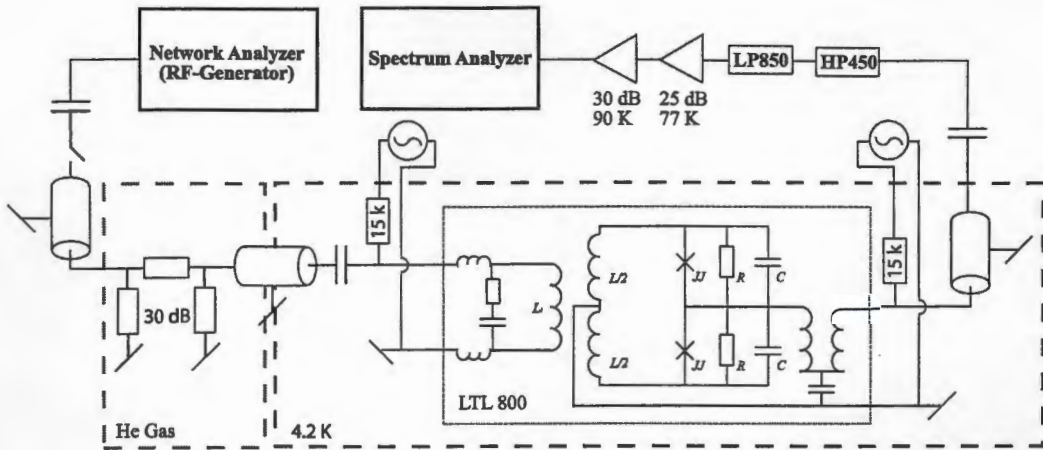
Figure 6.3: The noise temperature measurement schematics. The spectrum analyzer monitored the amplified Nyquist noise from the 30 dB attenuator. The network analyzer acted as a RF-signal generator for the gain calibration.

6.3 Noise Measurement

The simplified noise measurement setup is depicted in figure 6.3. We used the standard method of hot and cold resistor, to obtain the noise temperature of the SQUID amplifier. A 30 dB attenuator acted as a well defined 50 Ω source of Nyquist noise power. The attenuator was connected to the SQUID input through a 20 cm stainless steel coaxial cable, which enabled us to fix the attenuator either in liquid helium bath or in gas bath simply by lowering or rising the dip stick. The attenuator was in thermal contact with a heater and a diode, so that we could both change and measure the temperature of the attenuator in gas bath.

Two Miteq room temperature post amplifiers amplified the output signal. A low pass and a high pass Mini-Circuit filter had to be installed between the SQUID and the post amplifier to reduce interferences from the post amplifier. The amplified signal was read by Hewlett Packard E4407B Spectrum Analyzer.

The network analyzer acted as a radio frequency signal source for gain measurements. To avoid possible gain drifts, the total gain of the system was measured immediately after the noise measurements. In the gain measurement, −60 dBm microwave signal from Network Analyzer was fed through coaxial cables and a DC-block to the attenuator input. The total attenuation between the SQUID input and the network analyzer was measured to be 33.0 dB. The SQUID input signal was thus accurately known. The total gain of the system was then obtained by measuring the transmitted signal.

To minimize the 50 Hz noise, all DC signals were fed through twisted pairs.

To reduce noise in bias currents, the 15 kΩ resistors were inserted in the liquid helium bath. The resistors were soldered on the sample holder, and they had an additional function in forming a bias-T component with the DC-block capacitors.

Chapter 7

Results and Discussion

In this Chapter, we present and analyze the experimental and simulated results. First we review the DC current-voltage characteristics, and calculate some important parameter values from the plots. The power gain as a function of flux is considered in a separate section, since it brings up a feedback phenomenon. The network analyzer measurement results are then presented, and compared to the circuit simulation results. Finally, we calculate the input noise temperature.

7.1   Current-Voltage Characteristics

Figure 7.1 presents a typical measured current-voltage characteristics. The total series resistance from bias-T components and wiring was measured to be 3.30 Ω, and we have extracted it from the plots. Figure 7.1(a) shows voltage across the SQUID as a function of bias current and flux. Two voltage-current curves with different flux values are plotted in 7.1(b). Voltage across the SQUID is zero at the region in the middle of the plot, i.e. the SQUID is superconductive at small bias currents. If the current is larger than the critical current (2.26),

$$I_m = 2I_c \left| \cos\left(\frac{\pi\Phi}{\Phi_0}\right) \right|, \tag{7.1}$$

a voltage appears as predicted by equation (2.36):

$$V = \frac{R}{2}\left(I^2 - I_m^2\right)^{1/2}. \tag{7.2}$$

The corresponding analytical results are depicted in figure 2.3.

The voltage across the SQUID as a function of flux with several discrete bias currents is depicted in figure 7.1(c). As discussed in Chapter 2, the RC
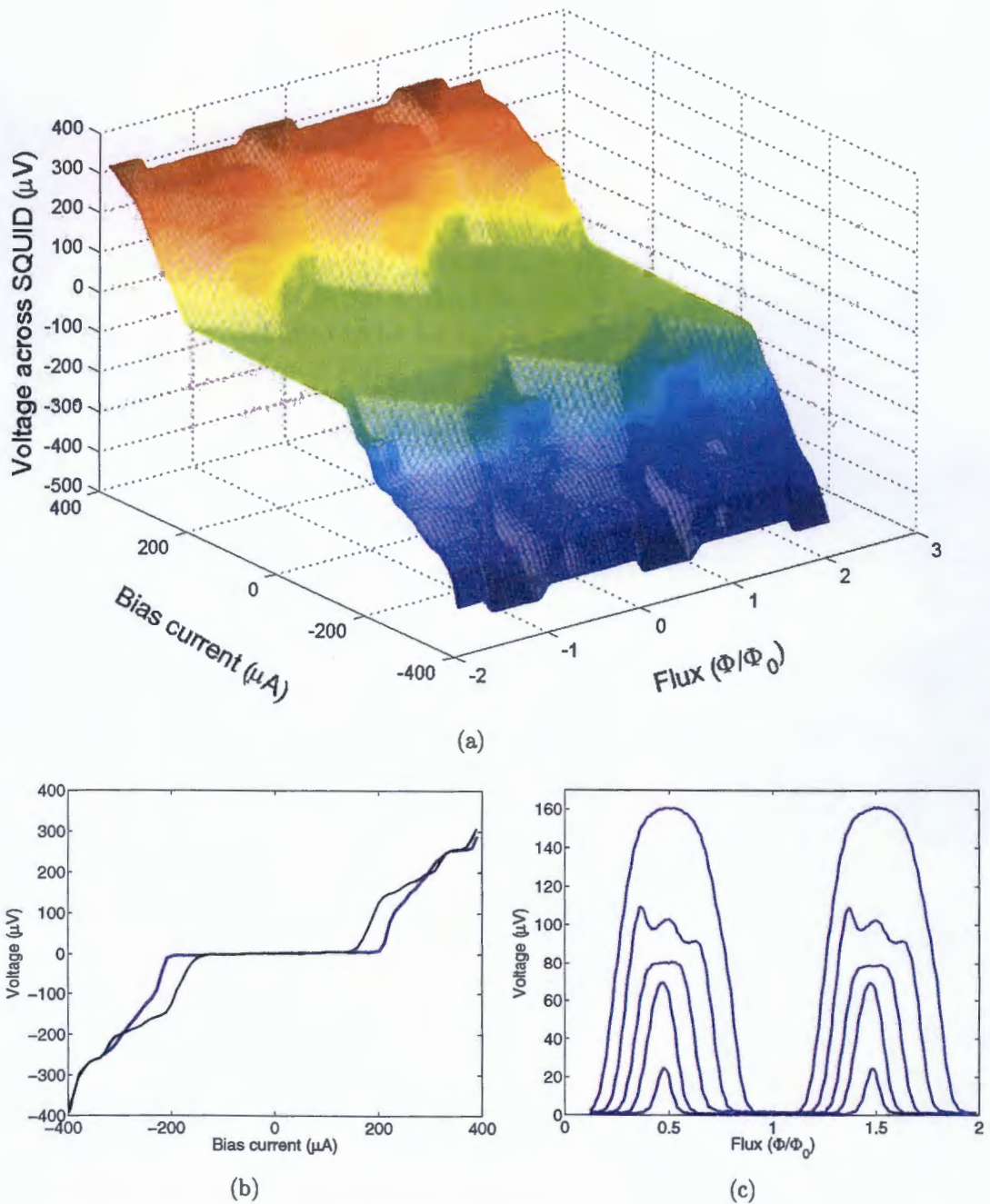
(a)

(b)

(c)

Figure 7.1: Typical current-voltage characteristics. (a) The voltage across the SQUID with respect to the bias current and the magnetic flux. (b) Two IV-curves obtained with different flux bias. (c) The voltage across the SQUID versus the applied flux with several bias current values.

shunt damps the input coil resonances, and the quarter wave microstrip resonance, which would appear at frequencies around 1 GHz, and 5 GHz, respectively. However, the washer resonance, predicted in Chapter 2 to 80 GHz, is not terminated. The curve is interfered at a bias voltage of about 90 μV corresponding to Josephson oscillations around 43 GHz, which is acceptably close to the washer resonance[1]. The washer resonance should not disturb the amplifier performance since the optimum voltage bias point is essentially less than 90 μV.

According to the figures, the maximum supercurrent is $I_m = 240 \pm 5$ μA, corresponding to junction critical currents $I_c = 120 \pm 5$ μA. For large values of the bias current, formula (2.36) reduces to Ohm's Law, from which the shunt resistances can be confirmed to be 2.7 Ω.

From the fundamental periodicity with respect to flux we can calculate the mutual inductance between the input coil and the SQUID loop: The flux applied to the SQUID loop is $\Phi = MI_f$, where I_f is the flux bias current. Thus the mutual inductance is just

$$M = \frac{\Phi_0}{\Delta I_f(\Phi_0)}, \tag{7.3}$$

where $\Delta I_f(\Phi_0)$ is the current change needed in order to add a single flux quantum in the loop. For 15 turn input coil, $\Delta I_f(\Phi_0)$ is 12.0 μA corresponding to mutual inductance of 129 pH. The SQUID loop inductance is then $L_s = M/n = 8.6$ pH.

7.2   Gain Versus Flux: The Feedback

The simultaneously measured voltage across the SQUID and power gain with respect to flux is shown in figure 7.2(c). The bias current was 107 μA, which maximizes the gain. The gain is much greater at the positive voltage-to-flux slope than at the negative slope, which is due to the feedback: the amplified voltage signal is coupled back to the input. If the flux-to-voltage transfer coefficient V_Φ is positive, the feedback is positive: the output voltage has the same sign as the input voltage, in which case the feedback signal amplifies the input signal, and thus the power gain. Correspondingly, the opposite sign of the flux-to-voltage transfer function causes negative feedback, which attenuates the input signal reducing gain.

---

[1]In fact, we can quite certainly attribute the interference at 90 μV to be due to the washer resonance. Since the SQUID loop inductance, and the junction capacitance are quite accurately known to be 8.6 pH, and 300 fF, we can obtain an estimation for the total parasitic capacitance from equation (3.9). The result is $C_p = 10$ pF, which is considerably larger than the total capacitance 1.6 pF calculated in Chapter 2. The models also imply that C_p may be somewhat larger than 2 pF.
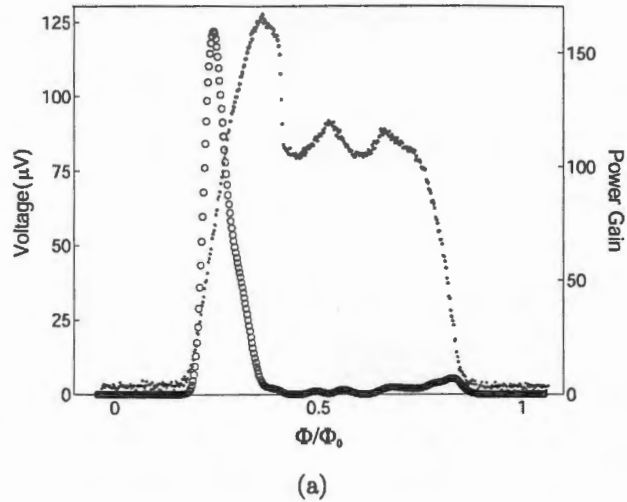
Figure 7.2: Simultaneously measured voltage and gain versus flux.

The amplified signal is fed back mainly through the parasitic capacitance between the input coil and the counter electrode (parameter C_{par} in the computer model). Additionally, because of the inductance between washer and ground arising from the microstrips on the chip and from the bond wire, the output current flowing between the washer and ground generates voltage across the washer, which may be fed back to the input via the input coil to washer capacitance [12].

In order to maximize the gain, some authors enforces the feedback by grounding the counter electrode instead of the washer [9–14], which is somewhat questionable since the feedback has several disadvantages. First of all, the amplifier may become unstable: the amplified output signal is fed back to the input, and thus the input signal is amplified repeatedly. Even if the amplifier with feedback is stable, it may not be linear, i.e. the gain depends on the amplitude of the input signal. Moreover, as will be seen in the next section, the feedback results in a large (over 10 dB) reflection coefficient $|S_{11}|$, which may be disastrous in some applications.

7.3   Network Analysis

A complete two port scattering parameter measurement was carried out for numerous operation points using a vector network analyzer. In this section, the main experimental results are presented, and compared to the results obtained from the circuit simulation model described in Chapter 5 using the parameter values given in table 5.1. The experimental plots are an average value of two to

four frequency sweeps. We selected 10 Hz IF bandwidth to diminish the noise floor.

In the section 7.3.1, we will describe the calibration methods, since the calibration has an essential role in the network analyzer measurements. The main results for LTL 800 are presented in section 7.3.2. In section 7.3.3 we will show that the feedback can be partially eliminated by reducing the inductance in the ground connection between input coil and the SQUID washer. The results obtained for LTL 800 with matched input impedance is shown in section 7.3.4.

7.3.1 Calibration

The filters, bias-T components, cables, and connectors introduces variations in magnitude and phase that mask the actual performance of the test device. The systematic error can be removed via calibration. In the calibration, the network analyzer measures the magnitude and phase responses of known standard devices, after which the network analyzer uses its internal vector math capabilities to remove the systematic errors from the measured test device data. The full two-port calibration provides vector error-correction for transmission and source match frequency responses. The two port calibration requires reflection and transmission measurements for both ports. In the reflection measurements, we used Agilent 85033 D Calibration Kit standards. The kit includes short, open and 50 Ω -load circuit terminations. In the transmission measurement, the two SMA cables were jointed together by a female-female connector. The calibration was made for frequencies from 100 to 1000 MHz, number of points were 1601, IF bandwidth was 100 Hz, and the test port power was -50 dBm.

The SQUID amplifier measurements were carried out in a liquid helium bath. The cryogenic temperature decreases the electrical length of the cables modifying, especially, the phase responses of the scattering parameters. To correct this minor systematic error, we made two additional calibration measurements in liquid helium bath, by measuring the S-parameters of open SMA connectors, and the cables connected by a female-female connector.

Figures 7.3(a)-(c) shows the responses for the open connectors at liquid helium bath. Ideally, S_{21} and S_{12} should be infinitely negative in decibels, since the signal should not transfer from one test port to the other. Of course, some finite values are obtained because of noise, but according to figure 7.3(a), the transmission coefficients are properly small, about -50 dB. From figure 7.3(b), the magnitudes of S_{11} and S_{22} are close to 0 dB, meaning that approximately all power is reflected, as expected. Phases of S_{11} and S_{22} shown in figure 7.3(c) increase linearly with frequency, which is because of the shortened electrical length of the
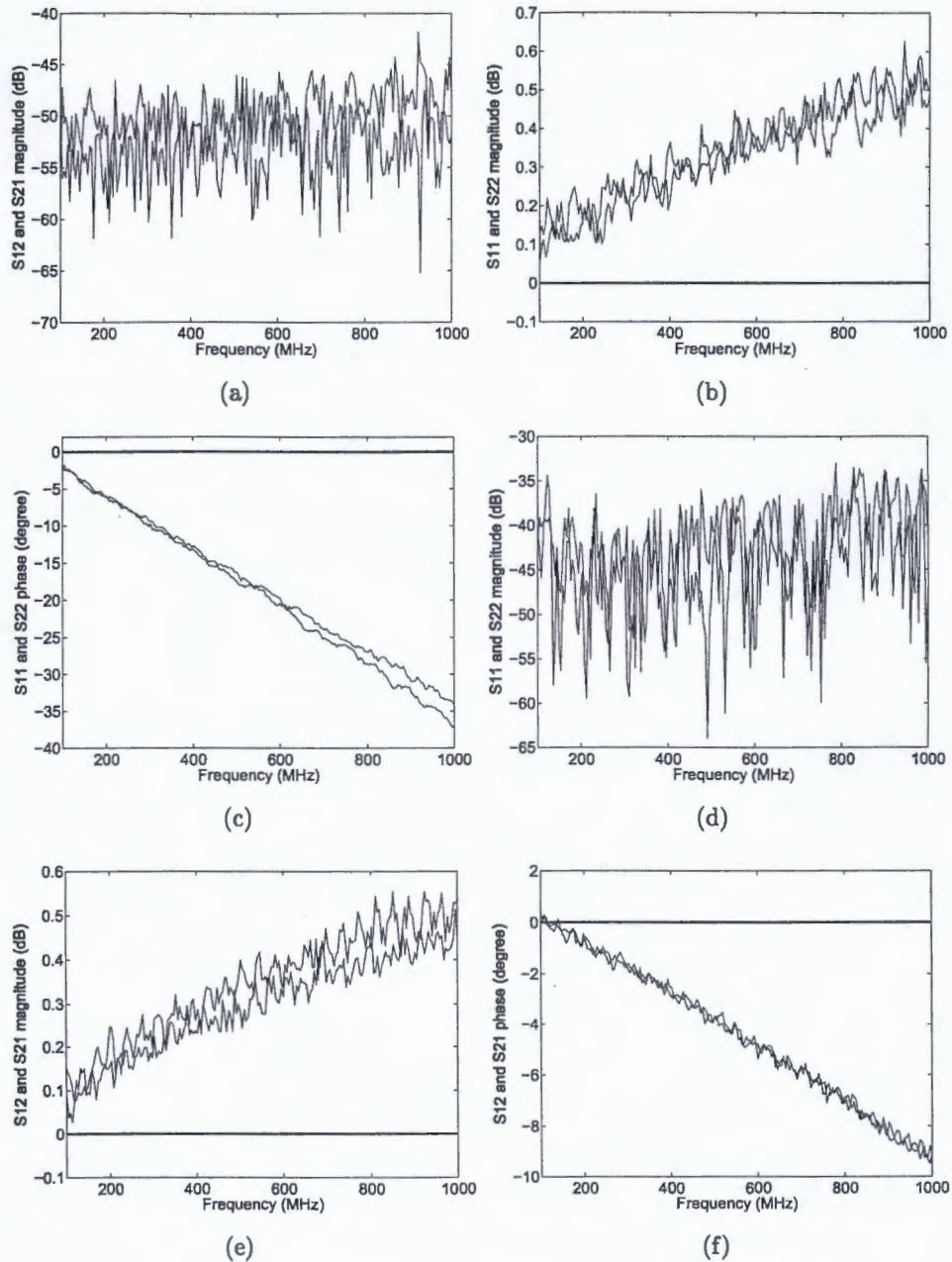
Figure 7.3: Low temperature calibration. Figures (a)-(c) are obtained for open cables, and (d)-(f) for cables connected together.
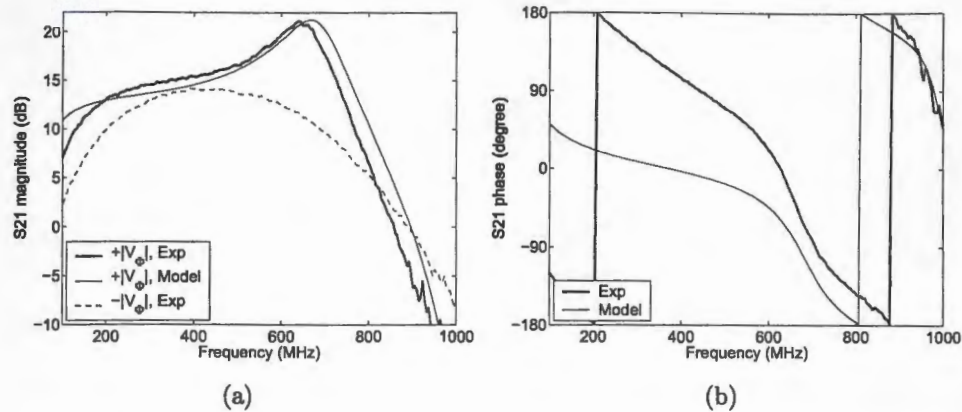
Figure 7.4: Measured and simulated frequency response for the gain S_{21}. (a) Magnitude in decibels. (b) Phase in degrees.

coaxial cables.

The measured responses of the cables at 4.2 K with shorted input-output connection is presented in figures 7.3(d)-(f). Now, the magnitudes of S_{11} and S_{22} are small, of order -40 dB, corresponding to negligible reflections. Again, there is some phase change due to the electrical length decrease.

The small deviations from ideal responses for S_{11} and S_{22} in figures 7.3(b) and 7.3(c), and for S_{12} and S_{21} in figures 7.3(e) and 7.3(f), was corrected straightforwardly from the test device data. The correction is mathematically exact if the transmission coefficients for open cables (figure 7.3(a)) , and reflection coefficients for connected cables (figure 7.3(d)), can be approximated to zero.

7.3.2 LTL 800 Network Characteristics

Figure 7.4(a) represents the magnitude of measured and simulated forward gain $|S_{21}|$ in decibels as a function of signal frequency. The corresponding phase response is plotted in figure 7.4(b). The gain measure for the negative current-to-flux transfer function is also plotted in figure 7.4(a), from which the feedback effect, described in previous section, is clearly seen.

The maximum gain is 22 dB at 630 MHz. The 3 dB bandwidth is exceptionally broad, about 150 MHz, which is due to the RC-shunt in the input circuitry. The gain-bandwidth product is much larger than found in literature for any SQUID amplifier operating in the same frequency range. Conventionally SQUID amplifiers have only a bandwidth of 50 MHz, which somewhat decreases their range of applications.

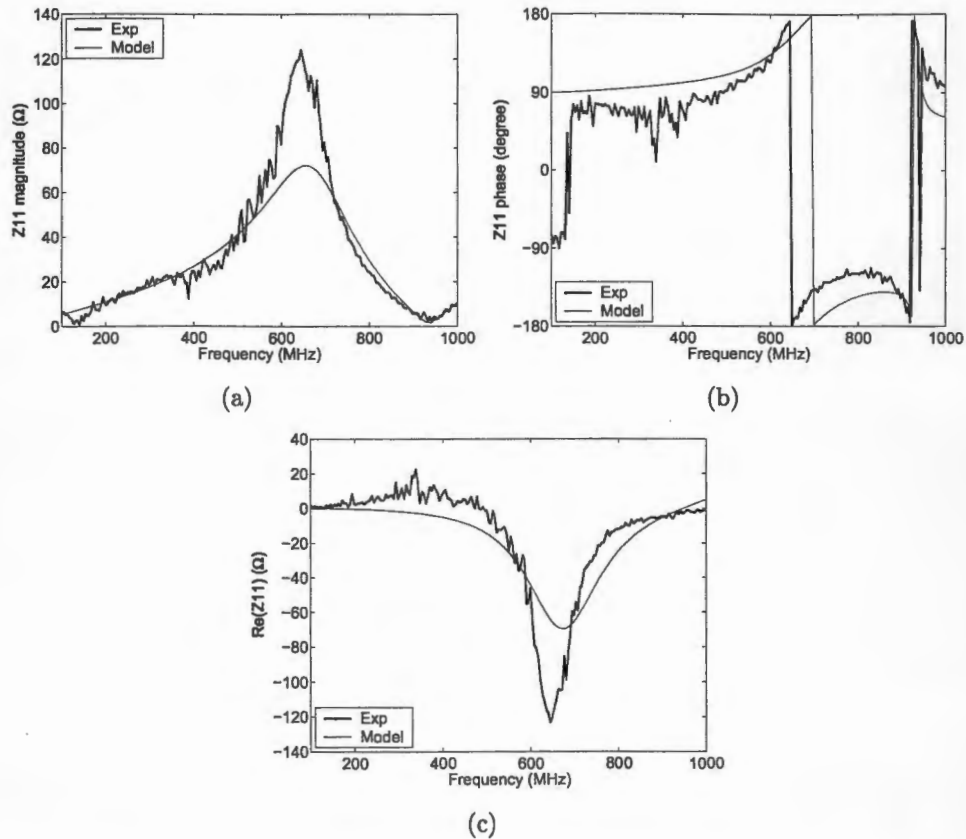Magnitude and phase of input impedance is shown in figures 7.5(a) and

Figure 7.5: Measured and simulated frequency response of input impedance Z_{11}. (a) Magnitude in Ohms. (b) Phase in degrees. (c) Real part in Ohms.

7.5(b). As discussed extensively in Chapter 4, the input coil inductance, the ground connection inductance, the stray inductances, and the parasitic capacitances causes a parallel resonance, which determines the operation frequency. The resonance is seen as a peak in the magnitude of the input impedance in figure 7.5(a). The series resonance at 920 MHz, formed by the stray inductances and the capacitances, limits the maximum operation frequency. At the series resonance, the input signal couples capacitively to the SQUID washer.

The real par of the input impedance at the operation frequency is about -120 Ω, as seen from figure figure 7.5(c). The negative impedance is due to the feedback: the amplified power coupled back to input exceeds the input power.[2]

The magnitude and phase of the output impedance is shown in figure 7.6.

---

[2]The analytical model considered in Chapter 4 excludes the feedback effect. The simulations in the chapter are compared to data measured for the negative flux-to-voltage curve, where the feedback is not prominent.
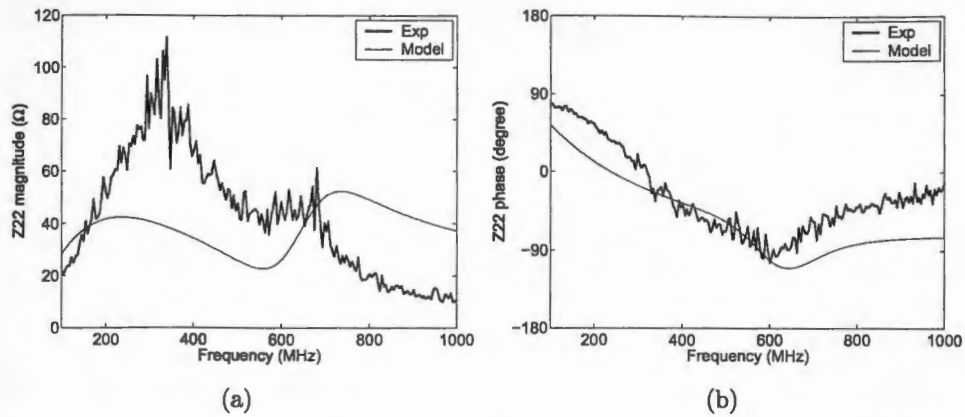
Figure 7.6: Measured and simulated frequency response of output impedance Z_{22}. (a) Magnitude in Ohms. (b) Phase in degrees.
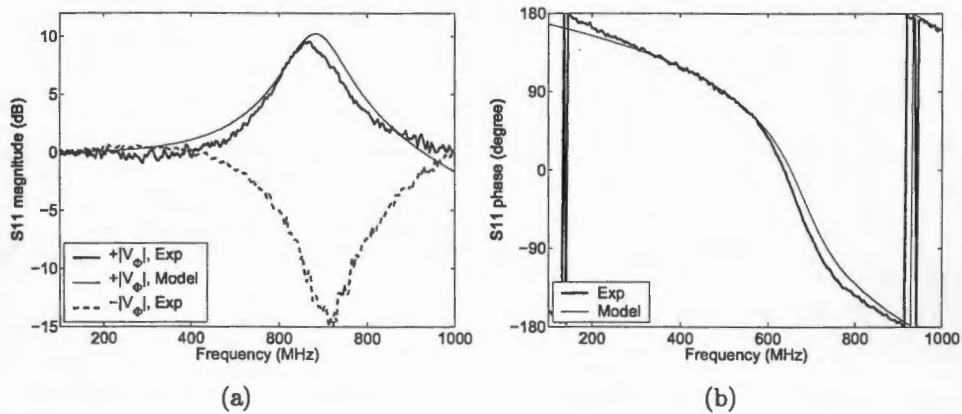

Figure 7.7: Frequency response of input reflection coefficient S_{11}. (a) Magnitude for the opposite slopes of the voltage-flux curve. Measured and simulated (a) magnitude in decibels, and (b) phase in degrees.

The experimental output impedance is close to 50 Ω at the optimum gain frequencies, i.e. the output is matched to the 50 Ω line. Hence, the output transformer seems to function properly.

The reflection coefficient S_{11} is shown in figure 7.7. The measured and simulated magnitude response in decibels is in subfigure 7.7(a), and corresponding phase response is in 7.7(b). Magnitude of the reflection coefficient is 10 dB at the operation resonance, which is another evidence of strong feedback. At the positive flux-to-voltage slope, the coupled signal is at the same phase, and hence the reflected signal is amplified. On the contrary, at the negative slope the feedback signal and the reflected signal repeal each other partially .
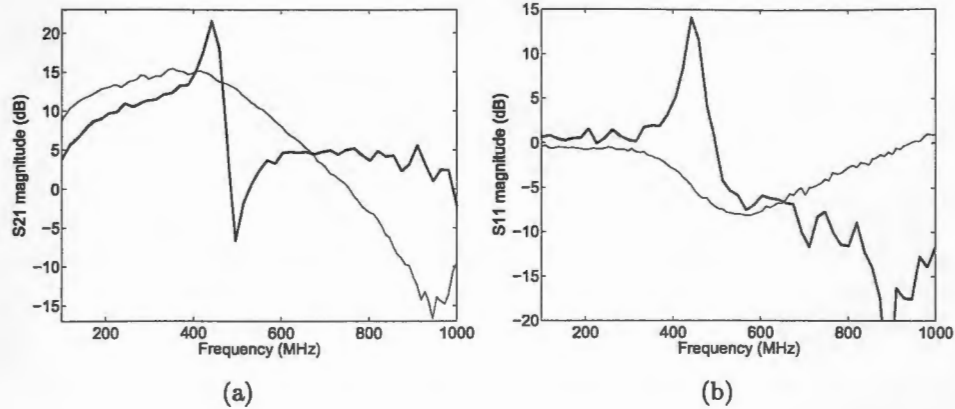
Figure 7.8: (a) Gain and (b) reflection coefficient measured with a large (thick line) and a small (thin line) ground connection inductance.

7.3.3 The Ground Connection Inductance

As mentioned in several context, there is significant inductance in the connection between the input coil the SQUID washer (parameter L_g in the Aplac model). The ground connection inductance can be reduced easily by bonding the grounded input and output pads together. In such a configuration, the ground connection inductance is determined by the inductance of the bond wire. The effect of ground connection inductance shown in figures 7.8(a) and 7.8(b) obtained for LTL 800 with 20 turn input coil. The thick lines are obtained without the bond wire, and the thin lines are obtained with 2 mm bond wire. The inductance of the wire is about 1 nH per mm [27]. The series resonance, seen as a downward peak in the frequency response of $|S_{21}|$ in figure 7.8(a), moves from 500 MHz (thick line) to 900 MHz (thin line) when the excessive inductance is reduced.

The most prominent impact of the diminished inductance is that it reduces the potential difference between the input coil and the washer, and thus the feedback (see section 7.2). The lack of feedback results in the diminished gain and reflection coefficient in figures 7.8(a) and 7.8(b), respectively. In order to avoid the feedback, we recommend that in the future SQUID designs, one end of the input coil is connected directly to the washer.

7.3.4 Matched Input Impedance

For optimum gain and noise performance, the input impedance of any amplifier should be matched to the characteristic impedance of the feed line. The impedance matching for a SQUID amplifier can be realized by the conventional
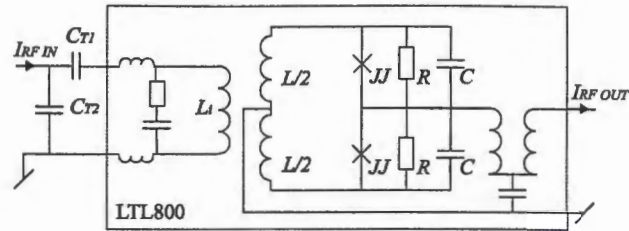
Figure 7.9: The input impedance was matched to the 50 Ω line using two capacitors, C_{t1} and C_{t2}.
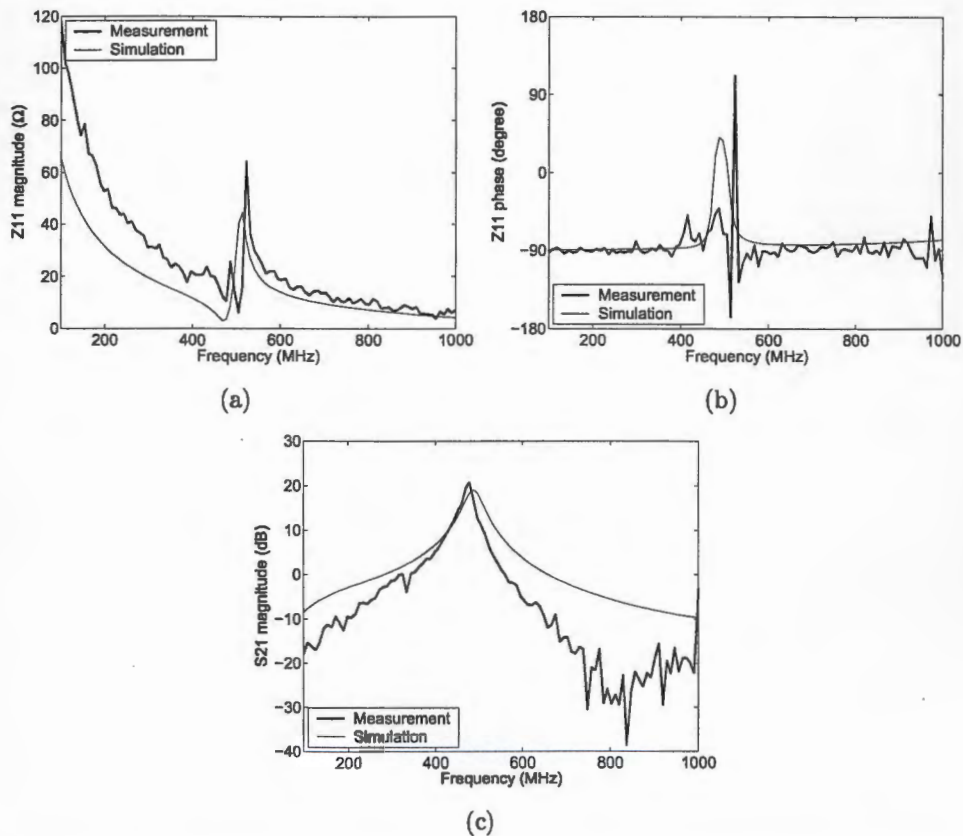

Figure 7.10: Measurement and simulation results for 20 turn LTL 800 with reactively matched input impedance. (a) Magnitude and (b) phase of the input impedance. (c) Magnitude of gain $|S21|^2$

methods of impedance matching. We used a resonant matching method with two reactive elements, as shown in figure 7.9. The two tuning capacitors were soldered into the sample holder. Capacitors $C_{T1} = 3.3$ pF and $C_{T2} = 10$ pF were selected with the help of the Aplac model.
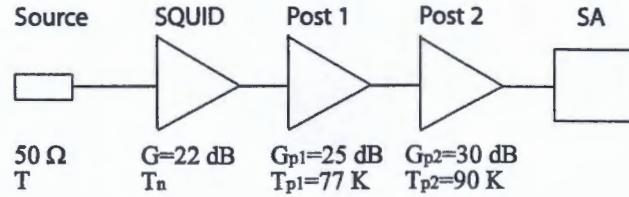
Figure 7.11: The block diagram for the SQUID noise temperature, T_n, measurement. The spectrum analyzer (SA) measured the noise signal amplified by two room temperature amplifiers.

Figures 7.10(a)-(c) present some measurement and simulation results obtained for the matched LTL 800 amplifier with 20 turn input coil. The magnitude and phase of the input impedance is plotted in figures 7.10(a) and 7.10(b). At the 500 MHz resonance, the input impedance is real and about 70 Ω, which is close to the characteristic impedance 50 Ω. Figure 7.10(c) shows the corresponding gain. The resonant matching leads to a narrow bandwidth in the order of 30 MHz.

7.4 Noise Performance

We obtained the noise temperature of LTL800 using the standard method of hot and cold resistor. The setup was described in Chapter 5. Figure 7.11 shows a simplified block diagram of the measurement. A resistor at temperature T generates white Nyquist noise power. We can easily write down the noise power at the second room temperature post amplifier output as

$$S(f) = GG_{p1}G_{p2}k_BT + GG_{p1}G_{p2}k_BT_n + G_{p1}G_{p2}k_BT_{p1} + G_{p2}k_BT_{p2}, \qquad (7.4)$$

where T_n, G, T_{p1}, G_{p1}, T_{p2}, and G_{p2} are the noise temperature and gain of the SQUID amplifier, and the first and the second post amplifier, respectively. Equation (7.4) predicts that the measured noise power depends linearly on the temperature of the resistor. This dependence is clear from figure 7.12, which shows the measured noise power as a function of the resistor temperature at 630 MHz. Extrapolating to $T = 0$ gives

$$T_n = \frac{S(f, T = 0)}{k_B GG_{p1}G_{p2}} + \frac{T_{p1}}{G} + \frac{T_{p2}}{GG_{p1}} \qquad (7.5)$$

The last term of the right hand side of equation (7.5) is negligible. The SQUID gain is 22 dB, and according to the manufacturer the noise temperature T_{p1} is 77 ± 5 K. The SQUID noise temperature is then 5.5 K. From equation (7.5) it is evident that the total gain $GG_{p1}G_{p2}$ has to be known accurately.
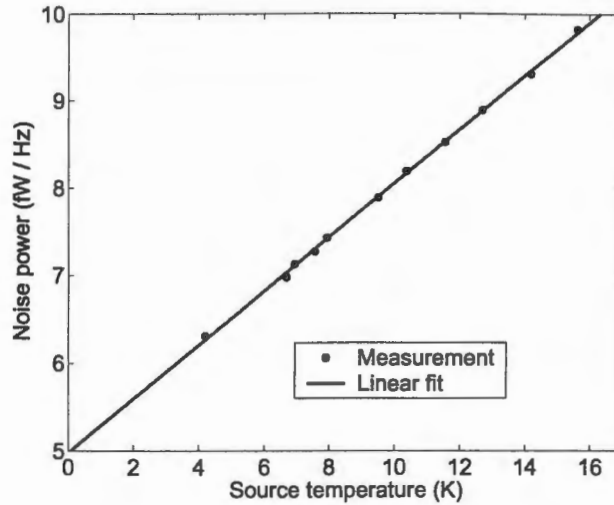
Figure 7.12: Amplified noise power at the spectrum analyzer input measured with various source temperature values.

From the linear fit, the 95% confidence bounds for T_n are 5.55 K and 5.46 K. In the measurement points where the resistor was in liquid helium bath, the dominating source of error was the spectrum analyzer and the post amplifiers. Otherwise, the main source of error was the temperature measurement. The diode was calibrated using a carbon resistance, but there may still be some systematic error in the temperature measurement. We estimated the maximum error in temperature to be less than 1 K, which results in another error of 0.5 K in the noise temperature.

Figure 7.13(a) shows the simulated noise temperature at 4.2 K as a function of frequency. The dotted curve is obtained directly from the Aplac simulation model. The noise in the model originates exclusively from the shunt resistors and the duplex filter, so that the model does not take into account the effect of down mixing of the high frequency noise. As discussed in Chapter 3, the mixing down effect can be included by a noise spectral coefficient of the order of 5, in which case we get the solid curve in the figure The simulated noise temperature is then 4 K at 650 MHz, which is reasonably close to the measured value. The obtained noise temperature is a decade larger than expected from analytical calculations. According to the Aplac model, the extra noise originates from RC-shunt.

The noise temperature of SQUID amplifier should reduce linearly with temperature, as discussed in Chapter 4, and e.g. in references [9, 14, 15, 20, 26]. The phenomenon is also shown in figure 7.13(b) obtained from the Aplac model. The bias current heats the shunt resistors, which limits the noise reduction. Neverthe-
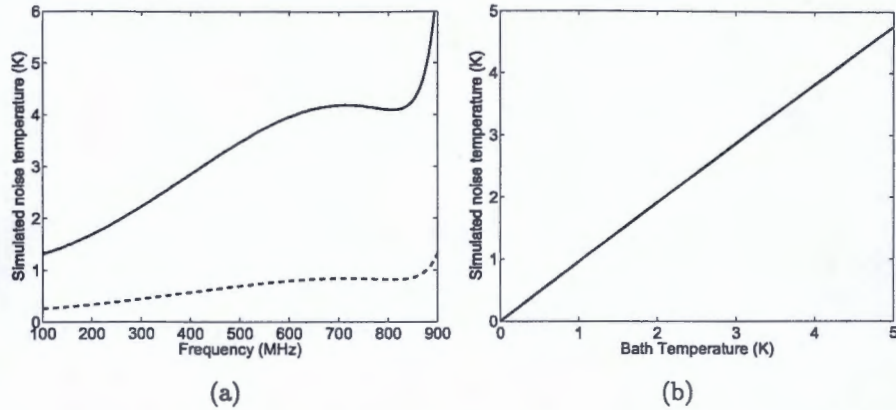
Figure 7.13: Simulated noise temperature. The dashed curve is obtained directly from the Aplac model. The solid curve takes into account the mixing down effect of high frequency noise. (b) The simulation predicts the usual linear dependence between the SQUID noise temperature and bath temperature.

less, it is possible to cool the shunt resistors down to 300 mK, and the RC-shunt resistor to 50 mK, in which case, according to the Aplac model, the LTL 800 noise temperature would be only around 150 mK, which is three times larger than the quantum limit.

Chapter 8

Concluding Summary

In this Master's Thesis, we characterized both experimentally and theoretically a state-of-the-art DC SQUID amplifier, LTL 800, designed to operate at microwave frequencies with quantum limited noise temperature. The operation principles of the device were studied by constructing an analytical model, and the experimental results were successfully explained by a detailed circuit simulation model. Both of the models will be applied for future SQUID amplifier designs.

The gain of LTL 800 SQUID amplifier was measured to be 22 dB at 630 MHz with 150 MHz bandwidth. The gain-bandwidth product, 24 GHz, is excellent, when compared with the results of the other manufacturers. However, the reflection coefficient was found to be large due to a significant feedback, which may be a problem in some applications.

The flux modulation curve was found to exhibit irregularities around 90 μV bias voltages due to the washer resonance. The optimum voltage bias point of the amplifier is about 30 μV, so that the washer resonance does not disturb the amplifier performance.

The experimentally determined noise temperature, 5.5 K, is order of magnitude higher than expected from analytic calculations. According to the computer simulation model, the excessive noise comes from the resistor-capacitor shunt terminating the input coil: the 3 pF capacitor may be too large to block the noise at signal frequencies. The measurements were carried out at liquid helium temperature (4.2 K). At 50 mK bath, the noise temperature is estimated to be 150 mK: only factor of three larger than the quantum limit.

References

[1] M. Mück, J.B. Kycia, and J. Clarke, *Superconducting quantum interference device as a near-quanum-limited amplifier at 0.5 GHz*, Appl. Phys. Lett. **61**, 967 (2001)

[2] S. Elliott, *The physics and chemistry of solids*, Jon Wiley & Sons Ltd,, (2000)

[3] M. Tinkham, *Introduction to superconductivity, 2nd ed.*, Dover Publications Inc. , (2004)

[4] T. Van Duzer, and C. W. Turner, *Superconductive devices and circuits, 2nd ed.*, Prentice-Hall, Inc. , (1999)

[5] D. M. Pozar *Microwave Engineering*, Jon Wiley & Sons Ltd, (1998)

[6] M.B. Ketchen and J.M. Jaycox, *Ultra-low-noise tunnel junction dc SQUID with a tightly coupled planar input coil*, Appl. Phys. Lett. **40**, 736 (1982)

[7] C. D. Tesche, and J. Clarke, *dc SQUID: Noise and Optimization*, J. Low Temp. Phys. **29**, 301 (1977)

[8] J. C. Gallop, *SQUIDS, the Josephson effects and superconducting electronics*, Adam Hilger , (1990)

[9] J. Clarke, M. Mück, and M-O. André ,*The microstrip DC SQUID amplifier*, NATO Sci. Ser. E, Appl. Sci. **375**, 473 (2002)

[10] M. Mück, and C. Welzel, *Superconducting quantum interference device amplifiers at gigahertz frequencies*, Appl. Phys. Lett. **82**, 3266 (2003)

[11] M. Mück, and J. Clarke, *Flux-bias stabilization scheme for a radio-frequency amplifier based on a superconducting quantum interference device*, Rev. Sci. Instrum. **72**, 3691 (2001)

[12] M. Mück, and J. Clarke, *The superconducting quantum interference device microstrip amplifier, Computing models*, J. Appl. Phys. **88**, 6910 (2000)

[13] M. Mück, M-O. André, and J. Clarke, *Microstrip superconducting quantum interference device radio-frequency amplifier, Tuning and cascading*, Appl. Phys. Lett. **75**, 3545, (1999)

[14] M-O. André, M. Mück, and J. Clarke, *Radio-frequency amplifier with tenth-kelvin noise temperature based on a microstrip direct current superconducting quantum interference device*, Appl. Phys. Lett. **75**, 698 (1999)

[15] P. Hakonen, M. Kiviranta, and H. Seppä, *Superconducting Electronics at mK Temperatures*, J. Low Temp. Phys. **135**, 823 (2004)

[16] R. H. Koch, D. J. Van Harlingen, and J. Clarke, *Quantum noise theory for the DC SQUID Amplifier* Appl. Phys. Lett. **38**, 380 (1980)

[17] M. A. Tarasov, V. Y. Belitsky, and G. V. Prokopenko, *DC SQUID RF Amplifiers*, IEEE Trans. Appl. Superconduct. **2**, 79 (1992)

[18] M. A. Tarasov, G. V. Prokopenko, and V. P. Koshelets, *Integrated rf amplifier based on dc SQUID*, IEEE Trans. Appl. Superconduct. **5**, 3226 (1995)

[19] T. Ryhänen, D. Drung, and H. Koch, *Design and optimization of DC SQUIDs fabricated using a simplified four-level process*, IEEE Trans. Appl. Magnetics **27**, 2927 (1991)

[20] T. Ryhänen, *Theoretical aspects, design, and characterization of dc superconducting quantum interference devices*, PhD thesis, Helsinki University of Technology, (1992)

[21] M. Sillanpää, L. Roschier, and P. Hakonen, *Inductive Single Electron Transistor*, Phys. Rev. Lett. **93**, 1 (2004)

[22] W. H. Chang, *The inductance of a superconducting strip transmission line*, J. Appl. Phys. **50**, 8129 (1979)

[23] C. Hilbert, and J. Clarke, *Signal and noise theory for a DC SQUID Amplifier* J. Low Temp. Phys. **61**, 263 (1985)

[24] C. Hilbert, and J. Clarke, *DC SQUIDs as radiofrequency amplifiers* J. Low Temp. Phys. **61**, 263 (1985)

[25] M. Mück, M-O. André, and J. Clarke, *Radio-frequency amplifier based on a niobium dc superconducting quantum interference device with microstrip input coupling*, Appl. Phys. Lett. **72**, 2885 (1998)

[26] M. A. Tarasov, and Z. Ivanov, *Optimization of input impedance and mechanism of noise suppression in a DC SQUID RF amplifier*, IEEE Trans. Appl. Superconduct. **6**, 81 (1996)

[27] A. Lehto, and A. Räisänen, *RF- ja mikroaaltotekniikka, 4. painos*, Otatieto Oy, (1994)